1976MNRAS.174..267C

Mon. Not. R. astr. Soc. (1976) **174**, 267–305.

A STUDY OF GALACTIC SUPERNOVA REMNANTS, BASED ON MOLONGLO–PARKES OBSERVATIONAL DATA

*D. H. Clark**

School of Physics, University of Sydney, NSW 2006, Australia

and

J. L. Caswell

Division of Radiophysics, CSIRO, PO Box 76, Epping, NSW 2121, Australia

(Communicated by R. L. F. Boyd)

(Received 1975 August 8; in original form 1975 January 8)

SUMMARY

Observations with the Molonglo and Parkes radio telescopes have recently produced improved radio frequency data for the southern galactic supernova remnants (SNRs). We have now used these observations to investigate the general evolutionary properties of SNRs—the first such large-scale analysis based on a near-homogeneous data set. Empirical relationships are derived which describe in general terms the expansion of SNRs, at least during the adiabatic phase of their evolution. An improved SNR distance scale is established, based largely on Parkes H I absorption measurements, and the resulting relationship between surface brightness and linear diameter for galactic SNRs is found to be compatible with that determined for the Magellanic Cloud SNRs, contrary to earlier conclusions.

Completeness in our catalogue down to a uniform level of surface brightness permits an improved estimate of the number of SNRs in the Galaxy and suggests that this number has previously been overestimated. We consequently infer a larger characteristic interval between supernova events (of a kind giving rise to typical radio remnants) of ~ 150 yr. Furthermore, on the assumption that most of the brighter SNRs are in the Sedov adiabatic expansion phase, the typical value of E_0/n (ratio of energy released in a supernova outburst to the number density of H atoms in the surrounding interstellar medium) implied by our data is 5×10^{51} erg cm^3, which is considerably higher than was commonly assumed in earlier work.

1. INTRODUCTION

Reviews investigating the general properties of galactic supernova remnants (SNRs) from a statistical analysis of observational data have been published by Milne (1970), Downes (1971) and Ilovaisky & Lequeux (1972a, b), and another such study of SNRs might at first appear unwarranted. However, a recent co-operative programme using high-resolution (~ 3 arcmin) observations from the Molonglo radio telescope at 408 MHz and observations of comparable resolution from the Parkes radio telescope at 5000 MHz has provided both a significant num-

* Present address: Mullard Space Science Laboratory, Department of Physics and Astronomy, University College London, Holmbury St Mary, Dorking, Surrey.

Downloaded from https://academic.oup.com/mnras/article/174/2/267/1052695 by guest on 20 August 2022

© Royal Astronomical Society • Provided by the NASA Astrophysics Data System

1976MNRAS.174..267C

TABLE I

A catalogue of 97 SNRs south of declination +18°

(1) Galactic source number	(2) Other catalogue number or name	(3) S_{408} (Jy)	(4) Reference	(5) S_{5000} (Jy)	(6) Reference	(7) α_{408}^{5000}	(8) Angular diameter (arcmin)	(9) Map reference	(10) Surface brightness Σ_{408} (W m^{-2} Hz^{-1} sr^{-1})
G193·3−1·5	PKS 0607+17	42*	25; Note 1				80	8	0·984E-21
G205·5+0·2	Monoceros	180*	25			(−0·5)	253	8	0·412E-21
G206·9+2·3	PKS 0646+06	8*	15				80	25	0·187E-21
G260·4−3·4	Puppis A	198	13	59	22	−0·48	47	13	0·134E-19
G261·9+5·5	PKS 0902−38	12*	2				40	16	0·112E-20
G263·9−3·3	Vela X, Y, Z	2300*	19			(−0·5)	256	8	0·526E-20
G287·8−0·5			Note 2				<42	17	
G290·1−0·8	MSH 11−61A	112	Revised	28	20	−0·55	12·6	28	0·106E-18
G291·0−0·1	MSH 11−62	22	Revised	9·2	12	−0·35	10·0	28	0·330E-19
G292·0+1·8	MSH 11−54	21	28	7·6	12	−0·41	5·4	28	0·108E-18
G293·8+0·6		9·0	6	2·1	6	−0·58	9·0	6	0·730E-20
G296·1−0·7		6·9	6			−0·7	16·0	6	0·404E-20
G296·5+10·0	PKS 1209−51	85*	31; interpolated	30	24	−0·45	81	31	0·194E-20
G296·8−0·3		15·0	4	3·2	4	−0·62	14·9	4	0·101E-19
G298·5−0·3		(7·4)	29		29	−0·36	3·7	28	0·793E-19
G298·6+0·0		(5·6)	29		29	−0·30	8·3	28	0·121E-19
G299·0+0·2		12·6	6	4·7	6	−0·39	10·5	6	0·171E-19
G302·3+0·7		7·5	6	3·0	6	−0·36	16·5	6	0·143E-20
G304·6+0·1	Kes 17	22	28	6·7	12	−0·48	6·9	28	0·693E-19
G308·7+0·0		16·7	6	7·0	6	−0·35	7·3	6	0·470E-19
G309·2−0·6		10	6	3·9	6	−0·37	12·6	6	0·945E-20
G309·8+0·0		26·4	6	7·4	6	−0·51	19·2	6	0·107E-19
G311·5−0·3		(5·7)	29	(1·7)	29	−0·48	3·9	28	0·548E-19
G315·4−0·3		15·9	6	4·9	6	−0·47	16·0	6	0·935E-20
[illegible]	RCW 86	86	4	18·3	4	−0·63	30	4	0·848E-20

© Royal Astronomical Society • Provided by the NASA Astrophysics Data System

Downloaded from https://academic.oup.com/mnras/article/174/2/267/1052695 by guest on 20 August 2022

1976MNRAS.174..267C

G316·3−0·0	MSH 14–57	37	28	16·7	24	−0·32	17·1	28	0·189E-19
G320·4−1·2	RCW 89, MSH 15–52	94	28	40	24	−0·34	25·8	28	0·212E-19
G321·9−0·3		18·3	6	7·8	6	−0·34	24·2	6	0·469E-20
G322·3−1·2	Kes 24	12·4	4; Note 3	1·3	4	−0·90	5·8	4	0·553E-19
G323·5+0·1		4·2	6	1·5	6	−0·41	10·8	6	0·540E-20
G326·3−1·8	MSH 15–56	180	7	98	20; Note 4	−0·24	36	7	0·208E-19
G327·1−1·1		10·6	6	4·3	6	−0·36	14·2	6	0·788E-20
G327·4+0·4	Kes 27	58	4	12·4	4	−0·61	21·0	4	0·197E-19
G327·6+14·5	SN 1006 A.D.	32·3*	21	7·7	21	−0·57	34	21	0·419E-20
G328·0+0·3		4·5	28	1	29	−0·55	6·4	28	0·165E-19
G328·4+0·2	MSH 15–57	20	28	11	12	−0·24	4·0	28	0·188E-18
G330·0+15·0	Lupus Loop	445*	21				368	21	0·493E-21
G330·2+1·0		8·6	6	4·0	6	−0·30	8·3	6	0·187E-19
G332·0+0·2		14·1	28		1	(−0·44)	12·0	28	0·147E-19
G332·4+0·1	MSH 16–51	40	28	11	12	−0·51	13·2	28	0·344E-19
G332·4−0·4	RCW 103	44	28	11	12	−0·55	9·4	28	0·747E-19
G335·2+0·1		27·1	6	8·6	6	−0·46	18·6	6	0·117E-19
G336·7+0·5		9·7	28	(1·4)	29	−0·37	9·9	28	0·145E-19
G337·0−0·1	CTB 33	26	28	(14·4)	29	−0·47	7·6	28	0·675E-19
G337·2−0·7		3·8	6	0·7	6	−0·67	3·9	6	0·375E-19
G337·3+1·0	Kes 40	24·6	4	7·2	4	−0·49	11·8	4	0·265E-19
G337·8−0·1	Kes 41	26	28	(7·2)	29	−0·51	10·6	28	0·347E-19
G338·2+0·4		(2·3)	29	(0·8)	29	−0·42	11·7	28	0·252E-20
G338·3−0·1		(12·5)	29	(2·4)	29	−0·66	8·2	28	0·279E-19
G338·5+0·1		(36·8)	29	(16·1)	29	−0·33	12·4	28	0·359E-19
G339·2−0·4		7·5	6	4·5	6	−0·20	9·9	6	0·115E-19
G340·4+0·4		8·2	6	2·9	6	−0·41	6·4	6	0·295E-19
G340·6+0·3		7·0	6	2·8	6	−0·36	4·9	6	0·437E-19
G341·9−0·3	MSH 16–48	7·4	4; Note 5	1·7	4	−0·59	6·1	3	0·300E-19
G344·7−0·1		4·7	6	1·3	6	−0·51	7·8	6	0·116E-19

© Royal Astronomical Society • Provided by the NASA Astrophysics Data System

Downloaded from https://academic.oup.com/mnras/article/174/2/267/1052695 by guest on 20 August 2022

1976MNRAS.174..267C

TABLE 1—*continued*

(1) Galactic source number	(2) Other catalogue number or name	(3) S_{408} (Jy)	(4) Reference	(5) S_{5000} (Jy)	(6) Reference	(8) α_{408}^{5000}	(8) Angular diameter (arcmin)	(9) Map reference	(10) Surface brightness Σ_{408} (W m^{-2} Hz^{-1} sr^{-1})
G346·6−0·2		14·9	6	4·3	6	−0·49	8·0	6	0·349E-19
G348·5+0·1	CTB 37A	97	7	39	20	(−0·33)	8·0	7	0·228E-18
G348·7+0·3	CTB 37B	34	7	22	20	(−0·30)	5·1	7	0·196E-18
G349·7+0·2		31	4	9·1	4	−0·49	1·7	30	0·156E-17
G350·0−1·8		49·5	6	13·6	6	−0·51	28·9	6	0·889E-20
G350·1−0·3		10·7	6	1·7	6	−0·73	4·1	6	0·964E-19
G351·2+0·1		8·1	6	3·1	6	−0·38	6·2	6	0·316E-19
G352·7−0·1		9·6	6	2·3	6	−0·57	6·4	6	0·347E-19
G355·9−2·5		12·3	6	3·4	6	−0·51	11·2	6	0·147E-19
G357·7−0·1	MSH 17–39	54·2	4	18·5	4	−0·43	5·2	30	0·301E-18
G4·5+6·8	Kepler's SN	33	18	7·1	20	−0·58	3·2	14	0·498E-18
G5·3−1·0	A4	38	7	27	23	−0·2	15·0	7	0·253E-19
G6·4−0·1	W28	460	28	179	26	−0·38	49	28	0·292E-19
G7·7−3·7		12·2	Unpublished	6·7	24	−0·25	19·5	Unpublished	0·481E-20
G10·0−0·3		1·9	28	(0·8)	29	−0·34	6·0	28	0·792E-20
G11·2−0·3		36	28	8·9	12	−0·56	4·2	30	0·306E-18
G11·4−0·1		9·4	6	2·8	6	−0·48	7·0	6	0·288E-19
G12·0−0·1		6·6	6	1·1	6	−0·71	5·4	6	0·339E-19
G15·9+0·2		7·7	6	1·9	6	−0·56	5·0	6	0·462E-19
G18·8+0·3	Kes 67	38	7	15	20	−0·36	15·0	7	0·253E-19
G21·8−0·6	Kes 69	110	28	28	12	−0·54	22·8	28	0·317E-19
G22·7−0·2		54	Revised			−0·57	24·6	28	0·134E-19
G23·3−0·3	W41, Kes 70	92	Note 6			−0·50	21·0	28	0·313E-19
G23·6+0·3		8·3	28		Note 7		7·2	28	0·240E-19
G24·7+0·6		27	28		11	(−0·59)	14·0	28	0·207E-19

© Royal Astronomical Society • Provided by the NASA Astrophysics Data System

Downloaded from https://academic.oup.com/mnras/article/174/2/267/1052695 by guest on 20 August 2022

1976MNRAS.174..267C

G24·7−0·6		12·3	6	3·6	6	−0·49	14·6	6	0·865E-20
G27·4+0·0	Kes 73	4·4	7; Note 8	1·4	20	−0·45	4·4	3	0·341E-19
G29·7−0·2	Kes 75	19·5	28	3·3	20	−0·71	2·4	28	0·512E-18
G31·9+0·0	3C 391	34·4	5	9·8	5	−0·57	4·8	30	0·224E-18
G32·0−4·9	3C 396.1		Note 9						
G32·8−0·1	Kes 78	12·8	4	7·7	4	−0·20	17·2	4	0·166E-19
G33·6+0·1	4C 00.70	35·5	4	7·8	4	−0·60	9·2	4	0·629E-19
G34·6−0·5	W44	299	7	149	20	−0·28	27·2	7	0·606E-19
G39·2−0·3	3C 396	30	28	8·8	24	−0·49	6·6	30	0·103E-18
G39·7−2·0	W50	>40	7; Note 10				>30	7	
G41·1−0·3	3C 397	29·8	4	8·7	4	−0·49	3·6	4	0·341E-18
G41·9−4·1	PKS 1920+06		Note 11			(−0·5)	164	25	0·169E-20
G43·3−0·2	W49B	53	28	16	12	−0·47	4·2	10	0·450E-18
G46·8−0·3		20·2	4	7·1	4	−0·42	15·6	4	0·124E-19
G47·6+6·1	CTB 63		Note 12				83·4	25	
G49·2−0·5	W51	200	27; Note 13			−0·25	26·6	27	0·424E-19
G53·7−2·2		11·7	7		32	(−0·32)	26·6	7	0·248E-20

* Not obtained from Molonglo pencil-beam survey.

References for Table I

1. Beard (1966)
2. Bolton, Gardner & Mackey (1964)
3. Caswell & Clark (1975)
4. Caswell, Clark & Crawford (1975)
5. Caswell *et al.* (1971)
6. Clark, Caswell & Green (1973, 1975a)
7. Clark, Green & Caswell (1975b)
8. Day, Caswell & Cooke (1972)
10. Downes & Wilson (1974)
11. Goss & Day (1970)
12. Goss & Shaver (1970)
13. Green (1971)
14. Gull (1975)
15. Haslam & Salter (1971)
16. Hill (1967)
17. Jones (1973)
18. Kesteven (1968a)
19. Milne (1968)
20. Milne (1969)
21. Milne (1971a)
22. Milne (1971b)
23. Milne & Dickel (1971)
24. Milne & Dickel (1975)
25. Milne & Hill (1969)
26. Milne & Wilson (1971)
27. Shaver (1969)
28. Shaver & Goss (1970a)
29. Shaver & Goss (1970b)
30. Slee & Dulk (1974)
31. Whiteoak & Gardner (1968)
32. Willis (1973)

© Royal Astronomical Society • Provided by the NASA Astrophysics Data System

Downloaded from https://academic.oup.com/mnras/article/174/2/267/1052695 by guest on 20 August 2022

1976MNRAS.174..267C

Notes to Table I

Note 1 Berkhuijsen (1974) has suggested that this source may form part of the Origem Loop ($\sim 5°$ diameter).

Note 2 Jones (1973) reported a strong non-thermal source, presumably an SNR, in front of the Carina nebula. The peak flux density of the source at his observing frequency of 30 MHz is 81 ± 8 Jy, and its diameter (equivalent gaussian) is <25 arcmin, which corresponds to <42 arcmin for a disc. If its angular diameter is >15 arcmin, it would be of too low a surface brightness to be seen on the 408 MHz Molonglo map of Shaver & Goss (1970a).

Note 3 Kes 24 has been classified as an SNR, although the possibility remains that the source could be extragalactic (Caswell, Clark & Crawford 1975).

Note 4 It is not clear whether a small-diameter (10 arcmin) non-thermal source lying near the centre of the (40 arcmin) SNR shell source is part of the same SNR. The observational data quoted in the table refer to both features, since they are not readily separated. Clark, Green & Caswell (1975b) give $\alpha_{\text{shell}} = -0{\cdot}4$ and $\alpha_{\text{central}} = -0{\cdot}1$.

Note 5 Note that this is the small-diameter source identified by Caswell & Clark (1975) as a possible SNR, and not the large region of diameter 30 arcmin originally suggested as an SNR (see e.g. Milne 1970).

Note 6 The 408 MHz flux density was estimated from the galactic survey described by Green (1972). In the estimate of flux density and size we excluded the northern feature G23·4−0·2, which appears to be thermal.

Note 7 By fitting gaussians to the brightness distributions, Shaver & Goss (1970b) derived $S_{408} = 10{\cdot}3$ Jy and $S_{5000} = 7{\cdot}4$ Jy. These give the flat spectral index of $-0{\cdot}13$, although it is noted that Shaver & Goss give a spectral index derived from the peak brightness temperatures of $-0{\cdot}34$. In the absence of further evidence there must remain considerable doubt as to whether this source is in fact an SNR.

Note 8 Note that this is the small-diameter source that Caswell & Clark (1975) suggest is an SNR, and not the complex of diameter 30 arcmin originally suggested as an SNR (see e.g. Milne 1969).

Note 9 Aizu & Tabara (1967) suggested that a large (1° diameter) feature of low surface-brightness may be an SNR. Milne & Hill (1969), and Caswell (1970a), summarizing the available evidence, supported an SNR classification. However, a bounded source is not evident on the 408 MHz survey of Haslam *et al.* (1974), and there must remain considerable doubt as to the SNR classification.

Note 10 The uncertain extent of this source made it impossible to estimate an exact 408 MHz flux density. However, the lower limit quoted does suggest a non-thermal classification for the source (*cf.* $S_{2700} = 28$ Jy, Velusamy & Kundu 1974).

Note 11 Milne & Hill (1969) have observed this large (2° diameter) source between 635 and 2700 MHz, estimating a non-thermal spectral index $\alpha_{635}^{2700} = -0{\cdot}5$ and S_{408} (extrapolated) = 305 Jy.

Note 12 This must remain a doubtful SNR classification. As noted by Milne & Hill (1969), this large (1° diameter) source of low surface brightness is located on a steep galactic background, and is confused with nearby sources. However, Caswell (1970a) has summarized the evidence supporting an SNR classification with $\alpha = -0{\cdot}5$.

Note 13 Although W51 is predominantly an H II complex, Shaver (1969) has recognized a background non-thermal shell with spectral index $-0{\cdot}25$.

ber of new SNR identifications (Clark, Caswell & Green 1973, 1975a), and greatly improved data for many known SNRs south of declination $+18°$ (Caswell, Clark & Crawford 1975; Clark, Green & Caswell 1975b). This programme, together with other investigations, has also confirmed that nearly 30 per cent of the sources previously classified as SNRs, and used by Ilovaisky & Lequeux in their study, had in fact been incorrectly classified (Shaver & Goss 1970b; Caswell 1972; Dickel

Downloaded from https://academic.oup.com/mnras/article/174/2/267/1052695 by guest on 20 August 2022

© Royal Astronomical Society • Provided by the NASA Astrophysics Data System

1976MNRAS.174..267C

& Milne 1972; Caswell & Clark 1975). In addition, a parallel programme of H I absorption measurements (Caswell *et al.* 1975) has recently provided a number of new SNR distances. It therefore seemed important to incorporate the improved data in a new statistical study of the general properties of SNRs.

A severe limitation of previous studies of this kind has been that they utilized inhomogeneous data from a large number of radio telescopes observing at different frequencies with differing sensitivities and beamwidths. In the present study we have restricted ourselves mainly to the use of 408 MHz data from the Molonglo radio telescope and 5000 MHz data with comparable resolution from the Parkes radio telescope. Results for individual remnants are of high quality and our study represents the first large-scale study of SNRs using a near-homogeneous data set. Furthermore, in the Molonglo survey a large fraction of the galactic plane has been searched to a uniform low-surface-brightness sensitivity limit, a fact which obviates for our study many of the difficulties associated with selection effects and incompleteness.

Our subsequent analysis concentrates on those aspects of SNRs where the above improvements have most effect.

2. OBSERVATIONAL DETAILS

The One-Mile cross-type radio telescope at the Molonglo radio observatory has been described by Mills *et al.* (1963); the half-power beamwidth of the individual pencil beams at 408 MHz is $2{\cdot}86 \times 2{\cdot}86 \sec(\delta + 35^\circ{\cdot}5)$ arcmin in right ascension and declination respectively. The results which we use are from the galactic survey $l\ 195^\circ \xrightarrow{360^\circ} 55^\circ$, $|b| \leqslant 3^\circ$, completed by the telescope between 1969 December and 1971 June (Green 1972, 1974) and from the earlier partial galactic survey by Shaver & Goss (1970a).

The Parkes 64-m radio telescope has a half-power beamwidth of ~ 4 arcmin at 5000 MHz. The SNR results used in the present paper are mainly from observations completed in 1968 May and August (Milne 1969; Goss & Shaver 1970), and in 1973 April (Clark *et al.* 1975a; Caswell, Clark & Crawford 1975). Observational details are given in the original references.

3. CATALOGUE OF SNRS

Green (1974) has recently published a comprehensive catalogue of galactic SNRs incorporating the corrections to earlier catalogues arising from the Molonglo–Parkes study. However, we found it necessary to reassess some of the flux densities and angular sizes in a more uniform approach. Our catalogue is given in Tables I and II. Table I lists the 97 known SNRs south of declination $+18^\circ$ (i.e. within the scope of the Molonglo survey) and gives Molonglo and Parkes observational data where available.

The table is composed as follows: column 1 gives the galactic source number of the SNR, and column 2, other catalogue numbers or common names; column 3 gives the 408 MHz integrated flux density estimate where available (estimates *not* obtained from the Molonglo pencil-beam survey are marked with an asterisk). In columns 3 and 5, flux densities in parentheses refer to estimates obtained by Shaver & Goss (1970b) from fitting gaussians to the individual source brightness distributions. Column 4 gives the original reference to the 408 MHz flux density and

© Royal Astronomical Society • Provided by the NASA Astrophysics Data System

Downloaded from https://academic.oup.com/mnras/article/174/2/267/1052695 by guest on 20 August 2022

1976MNRAS.174..267C

TABLE II

A catalogue of 23 SNRs north of declination +18°

(1) Galactic source number	(2) Other catalogue number or name	(3) References to experimental data	(4) S_{408} (Jy)	(5) Spectral index	(6) Reference	(7) Angular diameter (arcmin)	(8) Map references	(9) Surface brightness Σ_{408} (W m^{-2} Hz^{-1} sr^{-1})
G119·5+10·0	CTA 1	1	49*	$\alpha_{81}^{400} = -0.2$	1	130	1	0·435E-21
G120·1+1·4	Tycho's SN	7, 14, 22, 27, 34, 36	92	$\alpha_{750}^{5000} = -0.55$	22	7·9	34	0·221E-18
G130·7+3·1	3C 58	14, 22, 29, 36	38	$\alpha_{750}^{5000} = -0.1$	22	5·2	14	0·211E-18
G132·4+2·2	HB 3	1, 35	99	$\alpha_{38}^{2700} = -0.52$	35	72	35	0·285E-20
G160·5+2·8	HB 9	8, 15, 38	207*	$\alpha_{10}^{1420} = -0.44$	15	139	8	0·159E-20
G166·0+4·3	VRO 42.05.01	10, 15, 38	10*	$\alpha_{38}^{1400} = -0.40$	15	44	10	0·775E-21
G166·2+2·5	OA 184	9, 15, 38	17*	$\alpha_{38}^{1415} = -0.55$	15	76	9	0·441E-21
G180·0−1·7	S147	8, 15	101*	$\alpha_{178}^{960} = -0.5$	15	171	15	0·520E-21
G184·6−5·8	Crab nebula	22, 40	1303	$\alpha_{38}^{750} = -0.3$	22	5·2	40	0·723E-17
G189·1+2·9	IC 443	17, 18, 26, 29, 31	230	$\alpha_{38}^{5000} = -0.40$	31	40	17	0·216E-19
G54·4−0·3	HC 40	20, 6, 35	42	$\alpha_{178}^{2700} = -0.49$	6	43	35	0·341E-20
G55·7+3·4		4, 13, 28	1·6	$\alpha_{178}^{2700} = -0.5$	4	17·4	13	0·793E-21
G65·7+1·2	DA 495	38	11	$\alpha_{610}^{2700} = -0.64$	38	18·6	38	0·477E-20
G74·0−8·6	Cygnus Loop	21, 24, 32	316	$\alpha_{38}^{960} = -0.45$	25	180	21	0·146E-20
G74·9+1·2	CTB 87	11	14	$\alpha_{178}^{5000} = -0.47$	11	6·5	11	0·479E−19
G78·1+1·8	DR 4, γ Cygni	16, 38, 30	(100)	$(\alpha_{2700}^{10800} = -0.65)$	30, 38	(12·2)	16	(0·101E-18)
G82·2+5·4	W63	37, 35	250	$\alpha_{610}^{2700} = -0.7$	35	77	35	0·642E-20
G89·0+4·7	HB 21	12, 23, 38, 19, 5	371	$\alpha_{38}^{5000} = -0.40$	38	100	23	0·556E-20
G93·2+6·7	4C(T) 55.38.1	3	11	$\alpha_{178}^{1400} = -0.37$	3	25·0	Unpublished	0·192E-20
G93·6−0·2	CTB 104A	3, 35, 41	50	$\alpha_{178}^{2700} = -0.35$	3, 35, 41	61	35	0·206E-20
G94·0+1·0	3C 434.1	3, 22, 38, 35	20	$\alpha_{38}^{2700} = -0.53$	38, 22	26·6	35	0·425E-20
G111·7−2·1	Cas A	22, 33, 34	6700 (AD 1964)	$\alpha_{38}^{750} = -0.76$	22	4·2	33	0·569E-16
G117·3+0·1	CTB 1	38, 39, 35	13	$\alpha_{610}^{2700} = -0.58$	38	30	38	0·211E-20

* Only these are values measured at 408 MHz; the remainder are derived indirectly from the spectrum.

© Royal Astronomical Society • Provided by the NASA Astrophysics Data System

Downloaded from https://academic.oup.com/mnras/article/174/2/267/1052695 by guest on 20 August 2022

1976MNRAS.174..267C

References for Table II

1. Caswell (1967)
3. Caswell (1970b)
4. Caswell & Goss (1970)
5. Crowther (1965)
6. Day, Caswell & Cooke (1972)
7. Dickel (1969)
8. Dickel & McKinley (1969)
9. Dickel & Yang (1965)
10. Dickel, McGuire & Yang (1965)
11. Duin *et al.* (1975)
12. Erkes & Dickel (1969)
13. Goss & Schwarz (1971)
14. Goss, Schwarz & Wesselius (1973)
15. Haslam & Salter (1971)
16. Higgs & Halperin (1968)
17. Hill (1972)
18. Hill (1973)
19. Hill (1974)
20. Holden & Caswell (1969)
21. Keen *et al.* (1973)
22. Kellermann, Pauliny-Toth & Williams (1969)
23. Kundu (1971)
24. Kundu & Becker (1972)
25. Kundu & Velusamy (1967)
26. Kundu & Velusamy (1969)
27. Kundu & Velusamy (1971a)
28. Kundu & Velusamy (1971b)
29. Kundu & Velusamy (1972)
30. Kundu, Velusamy & Hardee (1974)
31. Milne (1971a)
32. Moffat (1971)
33. Rosenberg (1970)
34. Strom & Duin (1973)
35. Velusamy & Kundu (1974)
36. Weiler & Seielstad (1971)
37. Wendker (1968)
38. Willis (1973)
39. Willis & Dickel (1971)
40. Wilson (1970)
41. Yang & Dickel (1965)

'revised' indicates that we have re-assessed earlier Molonglo data; column 5 gives the Parkes 5000 MHz integrated flux density estimate where available, and column 6 the original reference to this flux density; (references in parentheses cite other high-frequency data where Parkes 5000 MHz measurements are not available); column 7 gives the spectral index (defined by $S \propto \nu^{\alpha}$) between 408 and 5000 MHz for those sources with flux density estimates available at the two frequencies (values in parentheses indicate that data at other frequencies have been used); column 8 gives the mean angular diameter of the SNR, measured in a manner to be described in Section 5.1, from the map referenced in column 9 (where possible, Molonglo maps were used); and column 10 gives the 408 MHz surface brightness Σ_{408} calculated from

$$\Sigma_{408} = 1{\cdot}505 \frac{S_{408}}{\theta^2} \times 10^{-19} \text{ W m}^{-2} \text{ Hz}^{-1} \text{ sr}^{-1}, \quad (1)$$

where S_{408} is the 408 MHz flux density in jansky (1 Jy $\equiv 10^{-26}$ W m^{-2} Hz^{-1}) and θ the angular diameter in minutes of arc.

Flux density estimates quoted in Table I are accurate to about 10 per cent. The 408 MHz flux density scale used was that of Wyllie (1969), and the 5000 MHz scale is relative to an assumed flux density for Hydra A of 13·5 Jy.

For completeness, the 23 known SNRs north of declination $+18°$ are listed in Table II. Our study of SNRs is based principally on Molonglo–Parkes observations of 'southern' SNRs. However, we have used 'northern' SNRs to increase the sample size in those parts of our study where homogeneity is not so important; in particular for age and distance calibration. Table II is composed as follows: columns 1 and 2 give the galactic source number and any common name or other catalogue number; column 3 gives a list of references to recent observational data for each source; column 4 gives a 408 MHz flux density, derived in most cases from the spectral index information given in column 5 (referenced in column 6) combined with flux density estimates at other frequencies—only those flux density values

Downloaded from https://academic.oup.com/mnras/article/174/2/267/1052695 by guest on 20 August 2022

© Royal Astronomical Society • Provided by the NASA Astrophysics Data System

1976MNRAS.174..267C

TABLE III

Sources previously classified as possible SNRs, but rejected on present evidence

Galactic source number	Comments	Ref.
G283·3−1·0	Thermal spectrum	6
G284·2−1·8	Flat spectrum; see note 1	2
G284·6−0·2	Optical identification. Thermal spectrum	6
G289·1−0·4	Thermal spectrum	6
G295·2−0·7	Thermal spectrum	6
G307·6−0·3	H109α line. Thermal spectrum	1
G310·6−0·3	Thermal spectrum	2
G310·8−0·4	H109α line. Thermal spectrum	3
G333·0+0·8	H109α line. Thermal spectrum	1
G342·1+0·1	H109α line. Thermal spectrum	2
G348·2+0·3	Optical identification. Thermal spectrum	5
G355·3+0·1	H109α line	3
G359·4−0·1	Thermal spectrum	4
G0·9+0·1	Thermal spectrum	4
G8·5−0·3	H109α line	3
G13·4+0·1	H109α line. Thermal spectrum	2
G20·0−0·1	H109α line. Thermal spectrum	2
G21·5−0·9	Flat spectrum. See note 2	2
G24·5+0·2	H109α line	1
G27·3+0·0	Thermal spectrum	2
G35·6−0·0	H109α line. Thermal spectrum	2
G35·6−0·4	Thermal spectrum	2
G37·5−0·1	Thermal spectrum	6
G45·5+0·1	H109α line. Thermal spectrum	8
G69·9+1·5	H109α line	3
G74·8+0·6	H109α line	3
G78·3+2·5	H109α line	3
G78·5−0·1	H109α line	3
G78·9+3·7	H109α line	3
G78·6+0·8	Thermal spectrum	7
G79·8+1·2	H109α line	3
G118·1+5·0	H109α line	3

References

1. Caswell (1972)
2. Caswell & Clark (1975)
3. Dickel & Milne (1972)
4. Little (1974)
5. Milne *et al.* (1969)
6. Shaver & Goss (1970b)
7. Velusamy & Kundu (1974)
8. Wynn-Williams, Downes & Wilson (1971)

Notes

1. The detection of a source near this position at 30 MHz (Jones & Finlay 1974) suggests that G284·2−1·8 may be non-thermal; however, if an SNR is present, its parameters are very uncertain since the 408 MHz map (Caswell & Clark 1975) and a new 5000 MHz map (Milne & Dickel 1975) differ somewhat in detail and neither shows a distinct shell structure.

2. The nature of this source remains uncertain. Caswell *et al.* (1975) give a distance measurements suggesting that it may be a unique young subluminous SNR ($\Sigma_{408} = 5{\cdot}23 \times 10^{-19}$ W m^{-2} Hz^{-1} sr^{-1}) with a flat spectrum, but it has been excluded from our catalogue pending confirmation.

Downloaded from https://academic.oup.com/mnras/article/174/2/267/1052695 by guest on 20 August 2022

© Royal Astronomical Society • Provided by the NASA Astrophysics Data System

1976MNRAS.174..267C

marked with an asterisk are values measured at 408 MHz; column 7 gives the mean angular size measured (by applying the technique described in Section 5.1) from the map of the source with highest resolution available, referenced in column 8; and column 9 gives the 408 MHz surface brightness estimate calculated using equation (1).

Prior to Green (1974) and the present work, the most recent comprehensive catalogue of galactic SNRs was that of Ilovaisky & Lequeux (1972a). They listed a total of 116 sources which they believed to be SNRs. New observational data suggest that approximately 30 of these are probably not SNRs and we omit them from our present catalogue; they are listed in Table III (together with the basis of their rejection).

We now consider the completeness of our present catalogue (Table I), in the region covered by the Molonglo galactic survey.

For sources larger than the telescope beam area, Ω, the sensitivity limit is essentially one of surface brightness such that:

$$(\Sigma_{\min})_{408\text{MHz}} = S_{\min}/\Omega,$$

where $S_{\min}$ is the minimum detectable peak flux density. For the Molonglo Cross 11-beam observations, we have

$$S_{\min} = 0{\cdot}2 \times 10^{-26} \sec(\delta + 35^{\circ}{\cdot}5) \text{ W m}^{-2} \text{ Hz}^{-1}$$

(three times the rms noise) and

$$\Omega = 7{\cdot}8 \times 10^{-7} \sec(\delta + 35^{\circ}{\cdot}5) \text{ sr},$$

so that

$$(\Sigma_{\min})_{408\text{MHz}} \sim 3 \times 10^{-21} \text{ W m}^{-2} \text{ Hz}^{-1} \text{ sr}^{-1}.$$

However, this does not take account of the confusion of low surface brightness objects with the galactic background. Green (1974) has shown (see her Fig. 2) that the 408 MHz background temperature averaged over the galactic latitude range -3° to $+3^{\circ}$ is always greater than 100 K in the galactic longitude range $300^{\circ} \xrightarrow{360^{\circ}} 50^{\circ}$, and approaches 300 K near the galactic centre. A background temperature of 200 K corresponds to a surface brightness of $\sim 1{\cdot}2 \times 10^{-20}$ W m^{-2} Hz^{-1} sr^{-1} and variations of this amount on a scale of a degree or so may hinder discovery of SNRs with brightness as low as this. We therefore regard $1{\cdot}2 \times 10^{-20}$ W m^{-2} Hz^{-1} sr^{-1} as our effective surface brightness confusion limit. Sources of lower surface brightness, for example Vela and RCW 86, have been mapped with the Molonglo cross but these sources are in regions where the background temperature is unusually low. Towards the galactic centre, where the background temperature approaches 300 K, the surface brightness confusion problem becomes more acute. Additionally, some SNRs, particularly those of low surface brightness, are undoubtedly missed because of confusion with discrete H II region complexes. To estimate the number thus missed is difficult, since SNRs may preferentially occur in such regions.

Two additional observational limits may be mentioned:

(i) The scale height perpendicular to the galactic plane (z) of the distribution of SNRs within 6 kpc of the Sun is about 110 pc (Mills 1974; see also Section 9). Since the Molonglo galactic survey was limited to $|b| \leqslant 3^{\circ}$, SNRs greater than one scale height from the plane would have been detected only if they were at least 2 kpc from the Sun. However, galactic surveys with other instruments have searched

Downloaded from https://academic.oup.com/mnras/article/174/2/267/1052695 by guest on 20 August 2022

© Royal Astronomical Society • Provided by the NASA Astrophysics Data System

1976MNRAS.174..267C

to higher latitudes, so it is unlikely that many SNRs remain undetected because of this limitation.

(ii) The effect of limited angular resolution. Small-diameter non-thermal sources from the Molonglo survey were investigated as possible SNRs only when their angular diameter was larger than 2 arcmin (most smaller non-thermal sources are assumed to be extragalactic (e.g. Kesteven 1968a)). Thus at 20 kpc from the Sun, for example, SNRs could be identified from the Molonglo–Parkes survey only if they had linear diameters greater than ~ 12 pc.

If Cas A, Tycho's SNR and Kepler's SNR were removed to a distance of 20 kpc, their 408 MHz flux densities would be 150, 12 and 8 Jy respectively. Few if any undetected remnants as young (i.e. with as high surface brightness and as small linear diameter) as these can be present anywhere in the Galaxy. since in the large portion of galactic plane searched for small-diameter sources by Clark & Crawford (1974), apart from the SNR G349·7+0·2, only two sources, G307·1+1·2 and G21·0+2·0, have 408 MHz flux densities greater than 10 Jy. Even if both were SNRs (Milne (1970) has previously suggested G307·1+1·2 may be one), which seems unlikely, our omission of them does not greatly affect the degree of completeness of our SNR catalogue.

We conclude that in the longitude range $180° \rightarrow 360°$ (this ' half ' of the Galaxy is almost completely covered by the Molonglo–Parkes survey) our catalogue should be nearly complete down to our surface brightness confusion limit. The galactic distribution (Section 9) also supports the conclusion that, to this limit, we are seeing most SNRs, even on the far side of the Galaxy.

Nevertheless, there must be some incompleteness on account of our exclusion of doubtful flat-spectrum sources at least some of which might be expected to be SNRs. On the other hand, it is likely that a few misclassified (H II or extragalactic) objects remain in our list. The net effect is probably that the true number of SNRs slightly exceeds our listed remnants.

Later, in Section 6, we will discuss the effect on our conclusions if the true number of SNRs above our sensitivity limit were as great as 40 per cent larger than the number listed in our catalogue; this we regard as a generous overestimate of the sum total of all effects.

4. THE EVOLUTION OF SNRS—THEORETICAL

Although the spectrum and polarization of the radio emission from SNRs confirm that it is synchrotron radiation, there is no single satisfactory theory yet for the origin and evolution of the fields and particles. There is increasing evidence that these might be dominated by quite distinct physical processes at various stages of a remnant's evolution as the explosion energy is transferred to the supernova ejecta and heats the interstellar medium.

Woltjer (1970, 1972) has suggested that the dynamical evolution of an SNR shell may be conveniently divided into four phases, and this division has been adopted in most subsequent investigations (e.g. Ilovaisky & Lequeux 1972a; Rosenberg & Scheuer 1973; Gull 1973).

In *phase* 1 (the free-expansion phase) the properties of the original explosion are important. Gull has investigated a possible mechanism for radio emission in phase 1, and has suggested that instabilities at the interface between the ejecta and interstellar medium result in a region of high magnetic field which gives rise to a

Downloaded from https://academic.oup.com/mnras/article/174/2/267/1052695 by guest on 20 August 2022

© Royal Astronomical Society • Provided by the NASA Astrophysics Data System

1976MNRAS.174..267C

shell source of non-thermal radiation as relativistic particles diffuse through this field into the interstellar medium. In *phase* 2 (the adiabatic-expansion phase) the heated interstellar medium dominates. Shklovsky (1962) suggested that the expansion now resembles that of an adiabatic blast wave created by releasing energy (but no mass) at a point in a homogeneous gas. In *phase* 3 (the isothermal-expansion phase) radiative cooling losses are significant and a dense shell is expected to form, driven from behind by hot gas. Compressed interstellar magnetic fields and relativistic particles may give rise to non-thermal radiation from the dense region, as in the model of van der Laan (1962). In *phase* 4 (the extinction phase) the SNR loses its identity and merges with the interstellar medium. It is of interest only in so far as it contributes to the intensity of the galactic background emission, and transfers kinetic energy to the interstellar medium.

Analytical solutions are available for the various phases. Rosenberg & Scheuer (1973) and Chevalier (1974) have attempted numerical computation of the full dynamical development; this work has emphasized the uncertainties of assigning observed SNRs to one of the above phases, since the transitions between them are complex and with unknown time scales. Nevertheless, we will quote here the analytical solutions for phases 2 and 3, since we have cause to refer to them later.

In phase 2 the adiabatic expansion is described by the similarity solution discussed by Sedov (1959)

$$D = 4{\cdot}3 \times 10^{-11} (E_0/n)^{1/5} t^{2/5}, \tag{2}$$

where D (pc) is the diameter of the remnant at time t (yr), E_0 (erg) is the energy released in the explosion and n (cm^{-3}) is the number density of H atoms in the surrounding medium. If the rate of supernova outbursts is assumed uniform, the number of SNRs with diameters less than D is proportional to the number of outbursts in a time $t(D)$ equal to the age of an SNR of diameter D, i.e.

$$N(<D) \sim t(D),$$

so that in phase 2, $N \sim D^{2{\cdot}5}$. (This is strictly true only if E_0/n is the same for all SNRs and if phase 1 is of negligible duration.)

In phase 3 each element of the shell may be considered to be moving with constant linear momentum. Woltjer (1972) then gives the variation of diameter of the remnant as

$$D \propto t^{1/4}, \tag{3}$$

and thus $N \sim D^{4{\cdot}0}$ for D (and hence t) so large that the preceding adiabatic phase is only a small fraction of the total lifetime.

Whereas theoretical studies of the dynamical evolution of SNRs attempt to describe the variation of linear diameter, D (and related parameters), with time, t, elapsed since the outburst, it is the surface brightness Σ (as defined in equation (1)) which most easily lends itself to observational investigation. We postulate that the variation of this parameter with linear diameter and time may be approximated by the relationships

$$\Sigma = AD^{\beta} \tag{4}$$

$$\Sigma = Bt^{\gamma}. \tag{5}$$

These two expressions may be combined to give the relationship for variation of linear diameter with time

$$D = Ct^{\delta}, \tag{6}$$

Downloaded from https://academic.oup.com/mnras/article/174/2/267/1052695 by guest on 20 August 2022

© Royal Astronomical Society • Provided by the NASA Astrophysics Data System

1976MNRAS.174..267C

which can then be compared with theory. As already noted in equations (2) and (3), the predicted values of δ for adiabatic and isothermal expansion are $\frac{2}{5}$ and $\frac{1}{4}$ respectively.

While there are sufficient SNRs with good estimates of linear diameter to permit investigation of the Σ–D relationship (4), the shortage of reliable age calibrators makes the direct evaluation of the Σ–t relationship (5) or D–t relationship (6) difficult. For this reason we introduce the cumulative distribution,

$$N(\Sigma) = P\Sigma^{\xi}, \tag{7}$$

where N is the number of SNRs with surface brightness greater than Σ, and the analogous distribution:

$$N(D) = QD^{\eta}, \tag{8}$$

where N is the number of SNRs with diameter less than D. If a constant rate of supernova outbursts is assumed, then

$$N(\Sigma) = P\Sigma^{\xi} = t/\tau \qquad \text{and} \qquad N(D) = QD^{\eta} = t/\tau.$$

Thus the functional dependence of Σ or D on t may be found from the cumulative distributions and only the constant τ requires calibration using SNRs of known age and measured Σ or D. The above relationships have been used in a number of SNR studies, and equations (4)–(8) above are in the form adopted by Mills (1974). The equations are not independent, and with certain assumptions:

$$\eta = \xi\beta \tag{9}$$

$$\gamma = 1/\xi \tag{10}$$

$$\delta = 1/\eta = 1/\xi\beta. \tag{11}$$

In addition,

$$C = (B/A)^{1/\beta} \tag{12}$$

and

$$Q = PA^{\xi}. \tag{13}$$

We would not expect to be able to identify a unique set of constants and exponents applicable throughout the lifetime of SNRs; indeed, we have already seen that theory predicts different forms of equations (6) and (8) for expansion during phases 2 and 3. However, in Section 7 a set of relationships will be presented which it is believed are applicable during phase 2 expansion provided that the phase 1 period is short.

5. THE Σ–D RELATIONSHIP FOR SNRS, $\Sigma = AD^{\beta}$

It has long been recognized (e.g. Shklovsky 1960a, b), that Σ_{ν} (the mean surface brightness at radio frequency ν) of an SNR is a particularly valuable observational parameter because it is distance-independent and, to a first approximation (see below), an intrinsic property.

After reaching a maximum value shortly after the birth of the supernova, Σ may be expected to decrease monotonically with time.* The outer diameter, D,

* It has been conjectured that in later phases, as different factors become important, an increase might occur; we shall show that there is no observational evidence for this.

© Royal Astronomical Society • Provided by the NASA Astrophysics Data System

Downloaded from https://academic.oup.com/mnras/article/174/2/267/1052695 by guest on 20 August 2022

1976MNRAS.174..267C

of the expanding SNR will *increase* monotonically with time. For various SNR models the variation of Σ with D may be predicted and compared with observation in the following ways:

(a) The current track of individual SNRs in the Σ–D plane may be found by measuring the secular decrease in flux density and the present rate of expansion.

(b) Using SNRs of known distance we may plot their distribution in the Σ–D plane to determine whether they follow a common evolutionary track.

If it appears from (b) that an evolutionary track is defined with not too much scatter, then this may be used in conjunction with measurements of Σ and *angular* diameter to determine the distances to SNRs for which no other distance information is available; since more than half of the known SNRs currently have no other distance measurement, the method is very valuable. Distance estimates for all SNRs are required to determine their distribution in the Galaxy, their spatial density and their rate of occurrence.

Recent investigations of the Σ–D relationship include those of Milne (1970), Downes (1971) and Ilovaisky & Lequeux (1972a) for galactic SNRs, together with those of Milne (1972) and Mathewson & Clarke (1973) for the Magellanic Cloud SNRs. It is usual to approximate the average evolutionary track by

$$\Sigma = AD^{\beta}$$

(i.e. equation (4)) and values of β so obtained have ranged from $-4{\cdot}54$ to $-3{\cdot}0$. In the various investigations Σ has been evaluated at frequencies as low as 408 MHz and as high as 5000 MHz.

5.1 *Measurement of the required observational parameters*

The required measurements are distances, d, to as many SNRs as possible together with the flux densities, S, and angular diameters, θ, for these distance calibrators; S and θ are also needed for sources at unknown distances in order to estimate their distances, using the Σ–D curve. Drawing on our later conclusion that $\Sigma \propto D^{-3}$ (approx.) we see that $d \propto S^{1/3}\theta^{-1/3}$ and is thus not very sensitive to errors in S or θ but is of course directly dependent on the distances to the calibrators. More generally $d \propto S^{1/\beta}\theta^{-(1+2/\beta)}$, and thus, for steeper Σ–D curves, distances are more dependent on θ and less on S: e.g. for $\beta = -4{\cdot}5$, $d \propto S^{-2/9}\theta^{-5/9}$. We now consider in turn the measurement of each parameter:

(a) *Flux density measurements.* These require a choice of frequency at which to obtain the intensity since the values of spectral index, α, differ for different SNRs. Furthermore there have been suggestions that the evolutionary track is a function of α (e.g. Shklovsky 1960a, b, 1968; Harris 1962) and that the spectral index may be a function of age (see Section 8); under such circumstances Σ_ν–D tracks depend on ν.

In order to check whether such effects are significant in the presence of other errors we have calculated S (and Σ) at both 408 and 5000 MHz.

(b) *Angular size measurements.* Where the boundary of a remnant is not circular, the area is the measured parameter and we define the equivalent diameter as $\theta = 2\sqrt{\text{area}/\pi}$. However, unless the source is an expanding sphere, the value of Σ is not a unique property of the source but is dependent on the orientation of the observer relative to the source. The ellipticity of typical remnants suggests

Downloaded from https://academic.oup.com/mnras/article/174/2/267/1052695 by guest on 20 August 2022

© Royal Astronomical Society • Provided by the NASA Astrophysics Data System

1976MNRAS.174..267C

TABLE IV

SNR distance calibrators

(1) Galactic source number	(2) Other names	(3) Distance (kpc)	(4) Mean linear diameter (pc)	(5) Reliability	(6) Remarks	(7) References
G184·6−5·8	Crab nebula	2·0	3·0	1	Optical radial velocity and proper motion	13
G189·1+2·9	IC 443	2·0	23		Optical	7
G205·5+0·2	Monoceros	1·0	74	2	Optical possible association	6
G263·9−3·3	Vela	0·5	37	2	Optical possible association	8
G290·1−0·8	MSH 11–61A	⩾3·4	⩾12·5		H I absorption, kinematic distance	4
G292·0+1·8	MSH 11–54	⩾3·7	⩾5·8		H I absorption, kinematic distance	3
G304·6+0·1	Kes 17	9·7	19·5	1	H I absorption, kinematic distance	3
G311·5−0·3		⩾6·6	⩾7·6		H I absorption, kinematic distance	3
G315·4−2·3	RCW 86; MSH 14–63	2·5	28	2	Optical possible association	14
G316·3−0·0	MSH 14–57	⩾7·2	⩾35·8	1	H I absorption, kinematic distance	3
G320·4−1·0	RCW 89; MSH 15–52	4·2	31·5	1	H I absorption, kinematic distance	3
G322·3−1·2	Kes 24	⩾20	⩾33·7	1	H I absorption, kinematic distance	3
G326·3−1·8	MSH 15–56	⩾1·5	⩾15·7		H I absorption, kinematic distance	3
G327·6+14·5	AD 1006	1·3	12·8		Optical from historical records	10
G328·4+0·2		⩾19·8	⩾28·9	1	H I absorption, kinematic distance	3
G332·0+0·2		⩾6·6	⩾23·0		OH absorption, kinematic distance	2
G332·4+0·1	MSH 16–51	⩾6·6	⩾25·4		OH absorption, kinematic distance	2
G332·4−0·4	RCW 103	3·3	9·0	1	H I absorption, kinematic distance	3
G337·8−0·1	Kes 41	⩾9·3	⩾28·7	1	H I absorption, kinematic distance	3
G348·5+0·1	CTB 37A	10·2	23·8	1	H I absorption, kinematic distance	3

© Royal Astronomical Society • Provided by the NASA Astrophysics Data System

Downloaded from https://academic.oup.com/mnras/article/174/2/267/1052695 by guest on 20 August 2022

G348·7+0·3	CTB 37B	10·2	15·1	1	H I absorption, kinematic distance	3
G349·7+0·2		18·3	9·0	1	H I absorption, kinematic distance	3
G357·7−0·1	MSH 17–39	⩾6	⩾9·1	1	H I absorption, kinematic distance	11
G4·5+6·8	Kepler	10	9·3	1	Optical and other considerations	7
G6·4−0·1	W28	⩾4·5(?)	⩾64(?)		Formaldehyde absorption, kinematic distance	16
G11·2−0·3		⩾5	⩾6·1		H I absorption, kinematic distance	11
G18·8+0·3	Kes 67	9·5	41·5	1	H I absorption, kinematic distance	3
G21·8−0·6	Kes 69	6·3	41·8	1	Formaldehyde absorption, kinematic distance	16
G29·7−0·2	Kes 75	⩾6·6	⩾4·6		H I absorption, kinematic distance	3
G31·9+0·0	3C 391	11±2·5	15·4	1	H I absorption, kinematic distance	11
G33·6+0·1		⩾7	18·7	1	H I absorption, kinematic distance	3
G34·6−0·5	W44	3	23·7	1	H I absorption, kinematic distance	3
G39·2−0·3		⩾11·3	⩾21·7	1	H I absorption, kinematic distance	3
G41·1−0·3	3C 397	⩾7·5	⩾7·9		H I absorption, kinematic distance	3, 11
G43·3−0·2	W49B	12±2	14·7	1	H I absorption, kinematic distance	11
G49·2−0·5	W51	4·1	31·7	1	H I absorption, kinematic distance	12
G74·0−8·6	Cygnus Loop	0·77	40	2	Optical	9
G111·7−2·1	Cas A	3·3	3·7	1	H I absorption, and optical	7
G120·1+1·4	Tycho	⩾6	⩾13·8	1	H I absorption, kinematic distance	5, 15
G130·7+3·1	3C 58	⩾8	⩾12·1	1	H I absorption, kinematic distance	5, 15
G132·4+2·2	HB3	2·0	42	2	Possible H II association. Revised	1

References for Table IV

1. Caswell (1967)
2. Caswell & Haynes (1975)
3. Caswell *et al.* (1975)
4. Goss *et al.* (1972)
5. Goss, Schwarz & Wesselius (1973)
6. Holden (1968)
7. Ilovaisky & Lequeux (1972a)
8. Milne (1968)
9. Minkowski (1958)
10. Minkowski (1966)
11. Radhakrishnan *et al.* (1972)
12. Sato (1973)
13. Trimble (1968)
14. Westerlund (1969)
15. Williams (1973)
16. Wilson (1972)

© Royal Astronomical Society • Provided by the NASA Astrophysics Data System

Downloaded from https://academic.oup.com/mnras/article/174/2/267/1052695 by guest on 20 August 2022

1976MNRAS.174..267C

that the variation of mean apparent angular diameter with orientation is sometimes as great as 10 per cent.

Practical measurements of angular size encounter the problems of limited angular resolution in the case of small-diameter sources on the one hand (case a), and limited sensitivity—i.e. poor signal-to-noise (or confusion) ratio—for low-surface-brightness (generally large-diameter) sources on the other hand (case b). In the best cases, the limited angular resolution causes only slight smearing of the boundary of the object, whereas in the worst cases a model source-intensity-distribution is necessary to interpret the slightly broadened instrumental response. Low sensitivity may result in the non-detection of a weak outer boundary of emission or, in worse cases, may be adequate to detect only a very small fraction of the total SNR giving a gross underestimate of its full extent. Fortuitously, both limitations can be overcome quite well for most sources owing to the characteristic intensity distribution of SNRs: most SNRs observed with both good sensitivity and high resolution show an intensity distribution which can be modelled quite well by a uniform disc with a superposed annulus of 'limb-brightening' and thus the true fall-off in intensity at the outer edge is quite steep. Our method of measuring angular size is as follows:

In case (b), for well-resolved sources, we use as the source boundary the half-intensity level up to the nearest ridge or plateau, with the additional proviso that such a boundary not be re-entrant but interpolated across any gaps in the 'disc'. Furthermore, where the sensitivity is high, we extend the boundary to a position one half-power beamwidth within the level of faintest detectable emission if this boundary is larger than that previously defined.

In case (a) (beam size $\gtrsim$ source size), the observed source half-intensity width θ_0 (corresponding to convolution of the source with the beam) may be deconvolved precisely if source and beam are assumed gaussian (with half-power diameters θ_G and θ_B respectively), so that

$$\theta_G^2 = \theta_0^2 - \theta_B^2.$$

If the beam is gaussian but the source has a disc intensity distribution, the diameter of the disc, θ_D, is approximately given by $\theta_D = 1{\cdot}67 \times \theta_G$.

We used the method of case (a) for $\theta_0 < 1{\cdot}25 \times \theta_B$ and that of case (b) for $\theta_0 > 1{\cdot}25 \times \theta_B$, since at this value they yield the same result.

The above procedure is objective in dealing with sources possessing irregular boundaries and is also insensitive to the resolution of the available observations (the estimated angular size of a remnant is therefore unlikely to change significantly even when much improved observations become available). Furthermore, these angular sizes should be compatible with those measured optically (with high resolution) in the Magellanic Clouds.

(c) *Distance measurements.* The need for more distance calibrators together with more reliable individual distance estimates has been the greatest limitation in studying the Σ–D relation to date. As Woltjer (1972) has remarked, the more dubious distance estimates are believed if they fit the Σ–D curve defined by more reliable calibrators, and rejected if they do not fit. Although this can be a useful criterion of whether a doubtful distance is actually in error, its application has caused a spuriously low scatter in previous Σ–D figures and an overestimate of the number of *independent* calibrators resulting in overconfidence in the correctness of the mean scale.

Downloaded from https://academic.oup.com/mnras/article/174/2/267/1052695 by guest on 20 August 2022

© Royal Astronomical Society • Provided by the NASA Astrophysics Data System

1976MNRAS.174..267C

The distance calibrators which we have considered are listed in Table IV, which includes many new calibrators from the recent H I absorption measurements by Caswell *et al.* (1975).

For many of the distances it is difficult to assess a realistic error. In a few instances a kinematic distance may be grossly in error if either the absorption feature used is spurious or if a feature corresponding to an even greater distance has not been detected; furthermore, some sources used as SNR distance calibrators may even prove to be extragalactic. It seems preferable to overcome this problem by using a large number of calibrators rather than by restricting the calibrators to a very few ' excellent ' ones, since the latter may not be typical anyway if the Σ–D relation intrinsically has a quite large scatter.

We have qualitatively estimated which are the more reliable distances (class 1 in Table IV) and have used these with equal weighting in the derivation of a best fit Σ–D relationship. The distances to some of these SNRs are strictly only lower limits but because they lie well to the right of the Σ–D plot we have used them as actual distances.

We note that the most recent Σ–D relation as used by Clark *et al.* (1973) utilized only nine calibrators, of which at least one (MSH 15–56) was assigned a distance which is not supported by subsequent observations. The distances to three of the others (G11·2−0·4, 3C 397 and Vela X) seem to be uncertain by large amounts and thus only five are retained in our new list of 24 ' class 1 ' calibrators.

5.2 *Discussion of the present Σ–D results and comparison with earlier discussions*

(a) *The derived slope.* The distribution of class 1 distance calibrators in the Σ_{408}–D plane is shown in Fig. 1(a). We first note that the distribution is consistent with Σ decreasing monotonically as D increases and there is a single essentially continuous distribution showing some scatter about a mean track. A least-squares fit in the range of surface brightness $2\times10^{-20}<\Sigma<5\times10^{-19}$ W m^{-2} Hz^{-1} sr^{-1} gave a slope of $-2{\cdot}7$, using only 20 ' class 1 ' calibrators and excluding RCW 103: this latter source apparently has a reliable distance but lies well to the left of (below) this line. Cas A, the Crab nebula and G349·7+0·2 were not used in the fit since their high values of Σ would have an unduly large influence. The range of Σ investigated is therefore quite small and the slope accordingly uncertain.

A slope of $-3{\cdot}0$ (in agreement with that for the Magellanic Clouds—see below), with a corresponding change in the constant of proportionality, provides an almost equally good fit. We subsequently adopt this latter relation since, in view of its uncertainty, the slope may be rounded to the nearest integer and it emphasizes that no clear difference exists between this Σ–D distribution and that for the Magellanic Clouds (Mathewson & Clarke 1973). If the calibrators are plotted in the Σ_{5000}–D plane we obtain the distribution of Fig. 1(b); the best-fit slope for the same 20 calibrators is $-3{\cdot}4$. We regard the difference as an indication of the uncertainty rather than as a significant change of slope with frequency; again, the slope of $-3{\cdot}0$ provides an almost equally good fit to the data. Furthermore at 5000 MHz there appears to be no reduction in the scatter of the points (relative to the 408 MHz plot), although we note that Cas A and the Crab nebula lie somewhat nearer to a common line if the relationship is extrapolated to higher surface brightness.

Most of the remaining less reliable calibrators are compatible with this relationship, if we bear in mind their uncertainties and the fact that many of their distances

Downloaded from https://academic.oup.com/mnras/article/174/2/267/1052695 by guest on 20 August 2022

© Royal Astronomical Society • Provided by the NASA Astrophysics Data System

1976MNRAS.174..267C

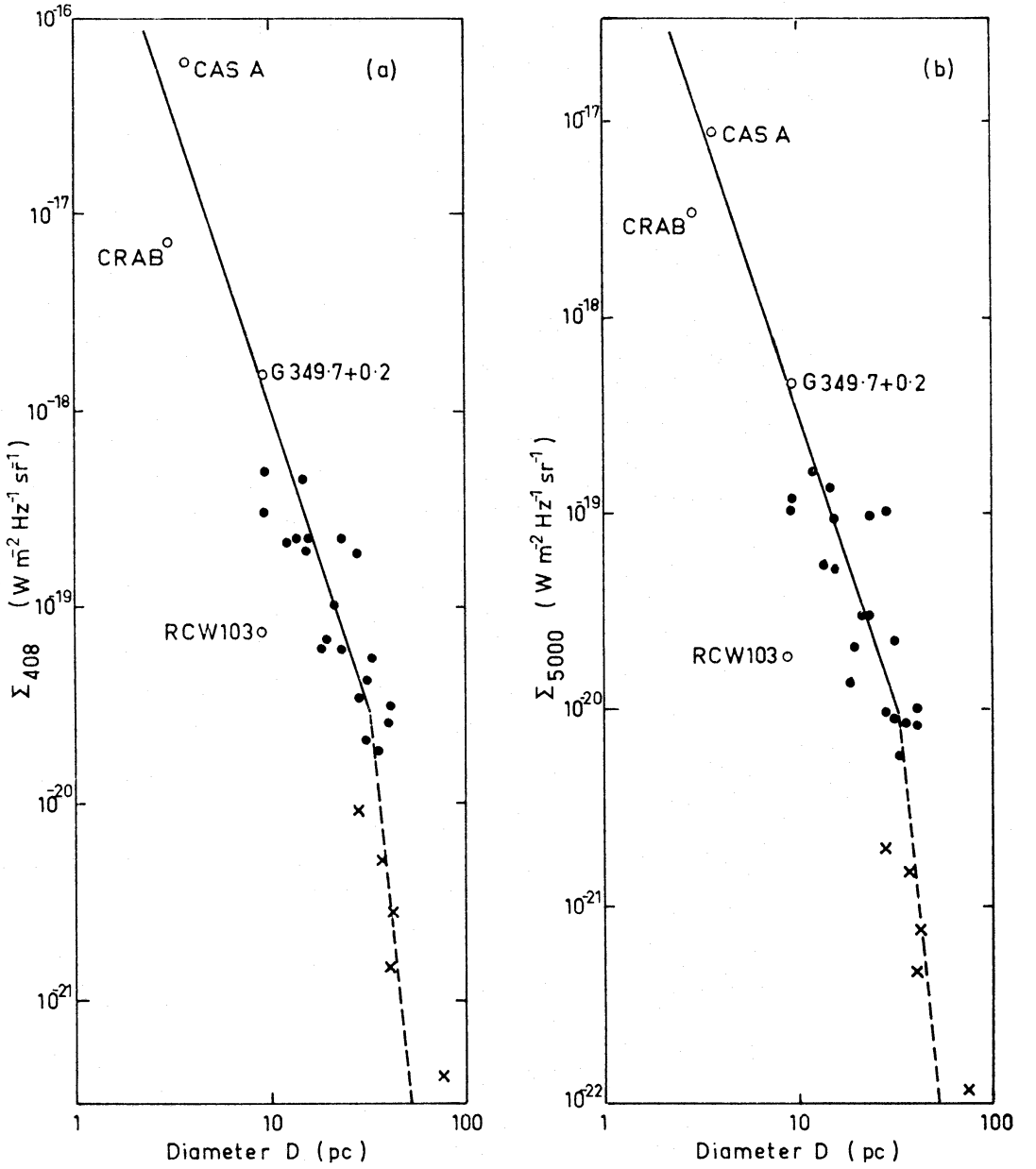

FIG. 1. *Surface brightness vs linear diameter: (a) at 408 MHz, (b) at 5000 MHz. The class 1 calibrators used to determine the solid line (adopted relationship) are shown as filled circles; the open circles, crosses and the broken line are explained in the text.*

are only lower limits. However, below $\Sigma_{408} = 10^{-20}$ W m^{-2} Hz^{-1} sr^{-1} there are five calibrators, all with distances of low accuracy (and designated class 2 in Table IV) of which none are kinematic distances, in contrast to the majority of the class 1 calibrators. These all lie well to the left of (below) the extrapolation of our $-3{\cdot}0$ slope, and while individually their distances are uncertain it seems significant that they all lie to the same side of the curve. In order to obtain distances more consistent with these calibrators, we suggest fitting a steeper slope to these fainter calibrators. As a compromise between a best fit to these calibrators and intersection with the line for brighter calibrators, we suggest steepening the slope to -10 at $\Sigma_{408} = 3 \times 10^{-20}$ W m^{-2} Hz^{-1} sr^{-1}, i.e. at $D \approx 32$ pc.

(b) *Distances derived from the Σ–D relation.* On the basis of the preceding

© Royal Astronomical Society • Provided by the NASA Astrophysics Data System

Downloaded from https://academic.oup.com/mnras/article/174/2/267/1052695 by guest on 20 August 2022

1976MNRAS.174..267C

investigation we will adopt the following Σ–D relationships. For

$$\Sigma_{408} > 3 \times 10^{-20} \text{ W m}^{-2} \text{ Hz}^{-1} \text{ sr}^{-1},$$

$$\Sigma_{408} = 10^{-15} D_{\text{pc}}^{-3}, \tag{14}$$

so that

$$d_{\text{kpc}} = 64{\cdot}6 \, (S_{408}\theta)^{-1/3},$$

whereas for

$$\Sigma_{408} < 3 \times 10^{-20} \text{ W m}^{-2} \text{ Hz}^{-1} \text{ sr}^{-1},$$

$$\Sigma_{408} = 3{\cdot}6 \times 10^{-5} D_{\text{pc}}^{-10}, \tag{15}$$

so that

$$d_{\text{kpc}} = \frac{94{\cdot}2}{\theta} \left(\frac{S_{408}}{\theta^2} \right)^{-1/10}.$$

(S_{408} is the 408 MHz flux density in Jy, and θ is the angular diameter in minutes of arc.) Using these relationships, and the observational data presented in Tables I and II, we have derived distances and related parameters for the SNRs. These values are given in Table V for the southern SNRs (based on Molonglo–Parkes observational data), and Table VI for the northern SNRs. In each table we list: the galactic source number (col. 1), the linear diameter, D, in pc, derived from the Σ–D relationship (col. 2), the distance from the Sun, d, in kpc (col. 3), the distance from the galactic centre, R, in kpc (col. 4), and the height above the galactic plane, z, in pc (col. 5). Those sources marked by an asterisk are of low surface brightness ($\Sigma < 3 \times 10^{-20}$ W m^{-2} Hz^{-1} sr^{-1}) and the Σ–D relationship (15) was used to determine their distance parameters whereas relationship (14) was used for the remaining sources. The derivation of the ages tabulated in column 6 will be discussed in Section 7.

We note that our distance scale is defined by the assumed distance of 10 kpc from the Sun to the Galactic Centre, used in the galactic rotation model. In contrast to conclusions based on earlier data (Milne 1972; Mathewson & Clarke 1973), we believe that our data show no evidence for a significant difference between galactic SNRs and those of the Magellanic Clouds and thus the two distance scales appear to be compatible. The improved agreement has resulted from additional galactic SNR distance calibrators from the work of Caswell *et al.* (1975). It has been suggested (e.g. Balona & Feast 1974) that the distance to the Galactic Centre should be reduced to perhaps 9 kpc, but the errors of this new determination do not yet warrant a change. The agreement with the Magellanic Clouds would be slightly poorer if this change were made, and earlier Σ–D investigations would show even greater discrepancies with the Magellanic Clouds.

For the 14 Magellanic Cloud remnants there is a range in diameter of a factor of ≈ 2 at a given surface brightness; this scatter almost certainly reflects an intrinsic scatter rather than measurement errors, since distance errors (of one source relative to another) must be negligible. In the case of the galactic SNRs we may assume that a similar intrinsic scatter is present; it may even be larger, since the optical technique used to recognize Magellanic Cloud SNRs may restrict the identifications to a subset with more uniform properties. In spite of this scatter the distances calculated from our Σ–D relationships are probably correct to within ~ 30 per cent for the majority of the SNRs.

(c) *The evolutionary significance of the* Σ–D *relation.* We first recapitulate the available information on the young SNRs Cas A and Tycho. If the fractional change

Downloaded from https://academic.oup.com/mnras/article/174/2/267/1052695 by guest on 20 August 2022

© Royal Astronomical Society • Provided by the NASA Astrophysics Data System

1976MNRAS.174..267C

TABLE V

Derived parameters for southern SNRs

(1) Galactic source number	(2) D (pc)	(3) d (kpc)	(4) R (kpc)	(5) z (pc)	(6) t (yr)
G193·3−1·5*	45·3	1·9	11·8	−50	
G205·5+0·2*	49·4	0·7	10·6	+2	
G206·9+2·3*	53·5	2·3	12·1	+92	
G260·4−3·4*	34·9	2·5	10·7	−148	
G261·9+5·5*	44·7	3·8	11·2	+365	
G263·9−3·3*	38·3	0·5	10·1	−29	
G290·1−0·8	21·1	5·8	9·7	−81	2452
G291·0−0·1	31·2	10·7	11·7	−19	6519
G292·0+1·8	21·0	13·4	13·4	+421	2423
G293·8+0·6*	37·1	14·2	13·7	+149	
G296·1−0·7*	39·3	8·4	9·8	−103	
G296·5+10·0*	42·3	1·8	9·3	+314	
G296·8−0·3*	35·9	8·3	9·7	−43	
G298·5−0·3	23·3	21·6	18·9	−113	3142
G298·6−0·0*	35·3	14·6	13·2	−11	
G299·0+0·2*	34·0	11·2	10·8	+39	
G302·3+0·7*	39·3	8·2	8·9	+100	
G304·6+0·1	24·3	12·1	10·4	+21	3490
G308·7+0·0	27·7	13·0	10·3	+11	4842
G309·2−0·6*	36·1	9·8	8·5	−103	
G309·8+0·0*	35·7	6·4	7·7	+6	
G311·5−0·3	26·3	23·2	18·2	−121	4253
G315·4−0·3*	36·2	7·8	7·0	−40	
G315·4−2·3*	36·5	3·2	8·1	−128	
G316·3−0·0*	33·7	6·8	6·9	−2	
G320·4−1·2*	33·3	4·4	7·2	−92	
G321·9−0·3*	38·8	5·5	6·6	−29	
G323·5+0·1*	38·2	12·2	7·3	+21	
G326·3−1·8*	33·4	3·2	7·5	−100	
G327·1−1·1*	36·8	8·9	5·4	−171	
G327·4+0·4*	33·6	5·5	6·1	+38	
G327·6+14·5	39·2	4·0	6·9	+1012	
G328·0+0·3*	34·2	18·4	11·2	+96	
G328·4+0·2	17·5	15·0	8·3	+52	1536
G330·0+15·0*	48·6	0·5	9·6	+131	
G330·2+1·0*	33·7	14·0	7·3	+244	
G332·0+0·2*	34·6	9·9	4·8	+34	
G332·4+0·1	30·7	8·0	4·7	+14	6261
G332·4−0·4	23·7	8·7	4·6	−61	3278
G335·2+0·1*	35·4	6·5	4·9	+11	
G336·7+0·5*	34·6	12·0	4·8	+105	
G337·0−0·1	24·6	11·1	4·3	−19	3599
G337·2−0·7	29·9	26·3	17·5	−321	5861
G337·3+1·0*	32·6	9·5	3·9	+166	
G337·8−0·1	30·6	9·9	3·8	−17	6210

Downloaded from https://academic.oup.com/mnras/article/174/2/267/1052695 by guest on 20 August 2022

© Royal Astronomical Society • Provided by the NASA Astrophysics Data System

1976MNRAS.174..267C

TABLE V—*continued*

(1) Galactic source number	(2) D (pc)	(3) d (kpc)	(4) R (kpc)	(5) z (pc)	(6) t (yr)
G338·2+0·4*	41·3	12·1	4·7	+84	
G338·3−0·1*	32·4	13·6	5·7	−24	
G338·5+0·1	30·3	8·4	3·8	+15	6059
G339·2−0·4*	35·4	12·3	4·6	−86	
G340·4+0·4*	32·2	17·3	8·6	+121	
G340·6+0·3	28·4	19·9	10·9	+104	5153
G341·9−0·3	32·1	18·1	9·1	−95	6999
G344·7−0·1*	35·4	15·6	6·5	−27	
G346·6−0·2	30·6	13·1	4·1	−46	6210
G348·5+0·1	16·4	7·1	3·2	+13	1300
G348·7+0·3	17·2	11·6	2·6	+61	1471
G349·7+0·2	8·6	17·4	7·8	+61	260
G350·0−1·8*	36·4	4·3	5·8	−135	
G350·1−0·3	21·8	18·3	8·6	−96	2660
G351·2+0·1	31·6	17·5	7·8	+30	6730
G352·7−0·1	30·6	16·5	6·7	−29	6210
G355·9−2·5*	34·6	10·6	0·9	−462	
G357·7−0·1	14·9	9·8	0·5	−16	1027
G4·5+6·8	12·6	13·5	3·6	+1602	676
G5·3−1·0*	32·7	7·5	2·6	−131	
G6·4−0·1*	32·3	2·3	7·7	−4	
G7·7−3·7*	38·7	6·8	3·4	−439	
G10·0−0·3*	36·8	21·1	11·4	−110	
G11·2−0·3	14·8	12·1	3·0	−63	1010
G11·4−0·1*	32·3	15·9	6·4	−28	
G12·0−0·1	30·9	19·7	10·1	−34	6363
G15·9+0·2	27·9	19·2	10·0	+67	4929
G18·8+0·3*	32·7	7·5	3·8	+39	
G21·8−0·6	31·6	4·8	5·8	−50	6730
G22·7−0·2*	34·9	4·8	5·9	−17	
G23·3−0·3	31·7	5·2	5·6	−27	6783
G24·7+0·6*	33·4	8·2	4·3	+86	
G24·7−0·6*	36·5	8·6	4·2	−90	
G27·4+0·0	30·8	24·1	15·9	+21	6312
G29·7−0·2	12·5	17·9	10·5	−62	662
G31·9+0·0	16·5	11·8	6·2	+6	1326
G32·8−0·1	34·2	6·8	5·6	−12	
G33·6+0·1	25·1	9·4	5·6	+16	3784
G34·6−0·5	25·4	3·2	7·6	−28	3898
G39·2−0·3	21·3	11·1	7·1	−58	2510
G41·1−0·3	14·3	13·7	9·0	−72	927
G41·9−4·1*	42·9	0·9	9·3	−62	
G43·3−0·2	13·0	10·7	7·7	−38	740
G46·8−0·3*	35·2	7·7	7·3	−40	
G49·2−0·5	28·7	3·7	8·1	−32	5290
G53·7−2·2*	41·3	5·3	8·1	−203	

* Σ–D relationship (15) was used for these low-surface-brightness sources; equation (14) was used for the remainder.

Downloaded from https://academic.oup.com/mnras/article/174/2/267/1052695 by guest on 20 August 2022

© Royal Astronomical Society • Provided by the NASA Astrophysics Data System

1976MNRAS.174..267C

TABLE VI

Derived parameters for northern SNRs

(1) Galactic source number	(2) D (pc)	(3) d (kpc)	(4) R (kpc)	(5) z (pc)	(6) t (yr)
G119·5+10·0*	49·2	1·3	10·7	+227	
G120·1+1·4	16·5	7·2	14·9	+176	1326
G130·7+3·1	16·8	11·1	19·2	+600	1387
G132·4+2·2*	40·7	1·9	11·4	+73	
G160·5+2·8*	43·2	1·1	11·0	+54	
G166·0+4·3*	46·4	3·6	13·5	+270	
G166·2+2·5*	49·1	2·2	12·1	+96	
G180·0−1·7*	48·3	0·9	10·9	−27	
G184·6−5·8	5·2	3·4	13·4	−344	
G189·1+2·9*	33·3	2·8	12·8	+144	
G54·4−0·3*	40·0	3·2	8·5	−17	
G55·7+3·4*	46·3	9·1	8·9	+540	
G65·7+1·2*	38·7	7·1	9·6	+149	
G74·0−8·6*	43·6	0·8	9·8	−120	
G74·9+1·2	27·2	14·4	15·2	+300	4646
G78·1+1·8	21·5	6·0	10·5	+188	2570
G82·2+5·4*	37·6	1·7	9·9	+160	
G89·0+4·7*	38·1	1·3	10·1	+107	
G93·2+6·7*	42·4	5·8	11·8	+678	
G93·6−0·2*	42·1	2·4	10·4	−8	
G94·0+1·0*	39·2	5·0	11·4	+87	
G111·7−2·1	2·6	2·1	10·9	−77	
G117·3+0·1*	42·0	4·7	12·8	+8	

* Σ–D relationship (15) was used for these low-surface-brightness sources; equation (14) was used for the remainder.

in flux density, $\Delta S/S$, and the fractional increase in angular diameter, $\Delta\theta/\theta$, for the same period are measured, then the value of β in $\Sigma = AD^{\beta}$ is given by

$$\beta = -2{\cdot}0 + \frac{\Delta S/S}{\Delta\theta/\theta}.$$

For Cas A, per year, we have $\Delta\theta/\theta = 0{\cdot}00333$ (van den Bergh & Dodd 1970) and $\Delta S/S$ has values between $-0{\cdot}007$ and $-0{\cdot}0129$, apparently depending systematically on frequency (Dent, Aller & Olsen 1974; see also Section 8).

Thus

$$\beta = -2{\cdot}0 - 7/3{\cdot}33 = -4{\cdot}1 \text{ at } 8000 \text{ MHz}$$

and

$$\beta = -2{\cdot}0 - 12{\cdot}9/3{\cdot}33 = -5{\cdot}87 \text{ at } 80 \text{ MHz}.$$

For Tycho, $\Delta S/S = -0{\cdot}008$ at λ 31·5 cm according to Stankevich, Ivanov & Torkhov (1973) and $\Delta\theta/\theta = 0{\cdot}0010$ according to van den Bergh (1971); an upper limit to $\Delta\theta/\theta$ is 0·0025 if uniform expansion has occurred since the outburst.

Thus $\beta = -2{\cdot}0 - 8{\cdot}0 = -10{\cdot}0$ apparently, or at least $\beta = -2{\cdot}0 - 8/2{\cdot}5 = -5{\cdot}2$ if the flux density decrease is correct but the measured angular expansion is not representative of the whole expansion.

Downloaded from https://academic.oup.com/mnras/article/174/2/267/1052695 by guest on 20 August 2022

© Royal Astronomical Society • Provided by the NASA Astrophysics Data System

1976MNRAS.174..267C

Immediate questions are whether Cas A is too young for its behaviour to be representative of any other SNR and whether the measurements on Tycho are sufficiently accurate. On purely theoretical grounds, even if we can decide whether an SNR is in phase 1, 2 or 3, the dependence of β on other factors does not allow a unique prediction of its expected value. It seems very important to check the results for Cas A and Tycho and to obtain similar data for Kepler, another young remnant of known age. It will also be important to determine whether all features decay at the same rate, since, if they do not, the decay over short periods may fluctuate about the value averaged over a longer interval. Alternatively, it is possible that the $-3{\cdot}0$ slope derived from the Σ–D plot does not represent the paths of individual remnants in the Σ–D plane; in particular Shklovsky (1968) suggested that if the slopes of some individual remnants are steeper, then the distribution at low surface brightness and small diameter could represent a sensitivity cut-off.

The use of the -3 slope in the subsequent interpretation (Section 7) should thus be treated with caution, whereas the use of this slope to derive approximate distance and diameter estimates depends only on the distribution of sources in the Σ–D plane not on their individual evolutionary tracks.

We particularly emphasize that the steepening of the Σ–D curve below $\Sigma = 3 \times 10^{-20}$ W m^{-2} Hz^{-1} sr^{-1} is uncertain and is proposed principally to allow more realistic distances to be estimated for low-surface-brightness remnants. However, in Section 7 we have explored the possibility that the change of slope is significant.

6. THE N–Σ RELATIONSHIP AND THE RATE OF OCCURRENCE OF SNRS

In Section 3 we argued that our catalogue of SNRs in the region covered by the Molonglo survey is essentially complete down to the surface brightness limit of

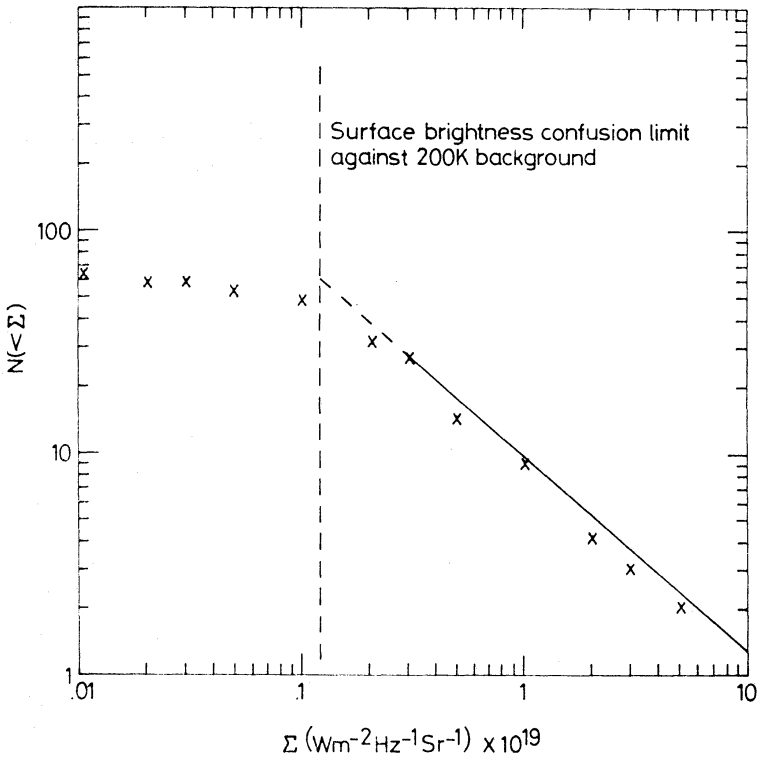

FIG. 2. *Cumulative distribution, N–Σ, for l 180° → 360°.*

Downloaded from https://academic.oup.com/mnras/article/174/2/267/1052695 by guest on 20 August 2022

© Royal Astronomical Society • Provided by the NASA Astrophysics Data System

1976MNRAS.174..267C

$\Sigma_{408} = 1{\cdot}2 \times 10^{-20}$ W m^{-2} Hz^{-1} sr^{-1}. The half of the Galaxy corresponding to longitudes 180° → 360° is almost completely covered to this limit. Accordingly we will determine the N–Σ relationship for this region, and, with the assumption of approximate symmetry about that galactic diameter which passes through the Sun, we double this relationship to obtain N–Σ for the whole of the Galaxy.

The N–Σ relationship for SNRs in the range 180° → 360° is shown in Fig. 2 by crosses (note that this includes three 'northern' SNRs from Table II). There is in Fig. 2 an apparent break in the derived function near $\Sigma \sim 10^{-20}$ W m^{-2} Hz^{-1} sr^{-1}. This break occurs near the surface brightness confusion limit discussed above, and is most likely an observational effect. However, in view of the Σ–D results obtained in Section 5, we impose a more stringent restriction and initially consider the function only for $\Sigma > 3 \times 10^{-20}$ W m^{-2} Hz^{-1} sr^{-1} (well above our surface-brightness confusion limit); here a power law fits the data with

$$N(>\Sigma) = 4{\cdot}2 \times 10^{-16}\, \Sigma^{-0{\cdot}86 \pm 0{\cdot}16}$$

(the slope of the function was estimated using the maximum-likelihood method of Crawford, Jauncey & Murdoch 1970). This relationship is shown in Fig. 2 by a solid line for $\Sigma > 3 \times 10^{-20}$ W m^{-2} Hz^{-1} sr^{-1} and is extrapolated to the surface-brightness confusion limit as a broken line.

The relationship for the whole of the Galaxy for $\Sigma > 3 \times 10^{-20}$ W m^{-2} Hz^{-1} sr^{-1} would then be

$$N(>\Sigma) = 8{\cdot}4 \times 10^{-16}\, \Sigma^{-0{\cdot}86 \pm 0{\cdot}16}, \qquad (16)$$

shown by the line in Fig. 3; the crosses in Fig. 3 show the experimental N–Σ data using all the SNRs from both Tables I and II (with the exception of the four which do not have satisfactory Σ measurements). The observations show a departure

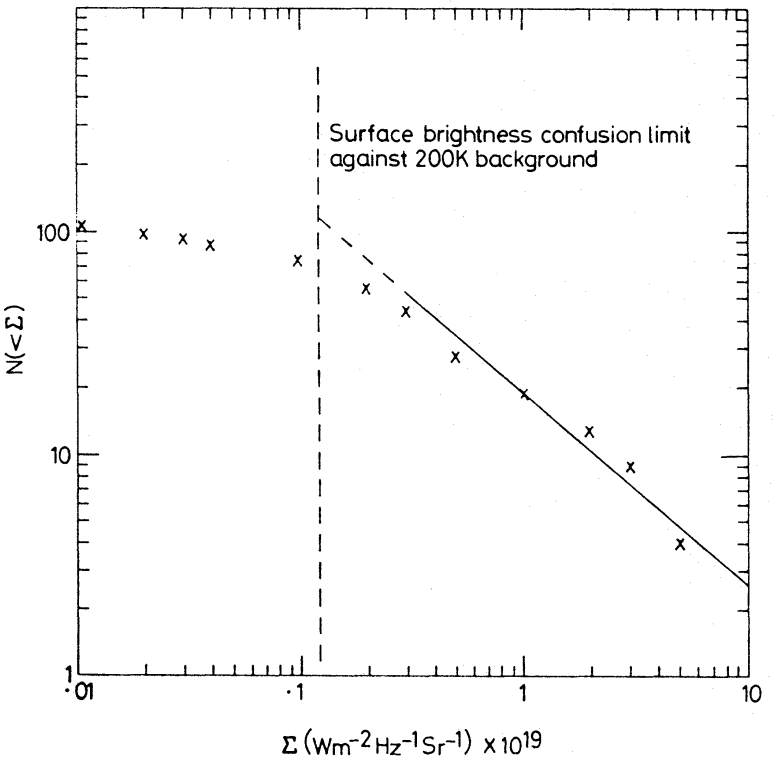

FIG. 3. *Cumulative distribution, N–Σ, for the whole of the Galaxy.*

© Royal Astronomical Society • Provided by the NASA Astrophysics Data System

Downloaded from https://academic.oup.com/mnras/article/174/2/267/1052695 by guest on 20 August 2022

1976MNRAS.174..267C

from the predicted line, equation (16), at a higher surface brightness than in Fig. 2, suggesting that there are still SNRs of moderately high surface-brightness in the range $l\,0° \rightarrow 180°$ that might be detected by northern observatories. For the range $l\,0° \rightarrow 180°$, relationship (16) suggests a deficiency of about eight in the number of SNRs (26) expected to have surface brightnesses greater than 3×10^{-20} W m^{-2} Hz^{-1} sr^{-1}.

To see the effects of any residual incompleteness in our catalogue, we write equation (16) as

$$N(\Sigma) = (1+f) \times 8{\cdot}4 \times 10^{-16}\, \Sigma^{-0{\cdot}86 \pm 0{\cdot}16},$$

such that the actual number of sources in the Galaxy is $(1+f)$ times the number catalogued, and obtain the $N(D)$–D relationship from this using our Σ–D relationship (equation (14)) which yields

$$N = (1+f) \times 6{\cdot}6 \times 10^{-3}\, D^{2{\cdot}56}.$$

(Note that this does not require that the Σ–D relationship be a well-defined evolutionary track but merely that the distance calibrators be representative of the whole population of SNRs in our catalogue.)

Since $N(D) = t/\tau$, where t is the time taken to expand to diameter D and τ is the mean interval between supernovae,

$$t/\tau = 6{\cdot}6 \times 10^{-3}\, D^{2{\cdot}56}(1+f),$$

i.e.

$$D = \tau^{-0{\cdot}39}[10^3\, t/6{\cdot}6(1+f)]^{0{\cdot}39}.$$

Estimates of τ may be obtained from SNRs of known age and diameter; however, it is instructive to note that, to within the errors, the form of our D–t relationship corresponds with the Sedov formula for adiabatic expansion,

$$D = 4{\cdot}3 \times 10^{-11}\, (E_0/n)^{1/5}\, t^{2/5}$$

(equation (2)). Thus, in order to see immediately the implications for E_0/n resulting from the choice of a particular value of τ, we modify slightly our experimental $N(D)$ fit by constraining the exponent to be 2·5 while retaining the value of $N = 26$ at $D = 25$. This gives

$$N = 8{\cdot}0 \times 10^{-3}\, D^{2{\cdot}50}(1+f); \tag{17}$$

thus

$$D = 6{\cdot}9[(1+f)\,\tau]^{-2/5}\, t^{2/5}. \tag{18}$$

Comparing this with the Sedov expansion formula (equation (2)) we have

$$\frac{E_0}{n} = \frac{1{\cdot}06 \times 10^{56}}{\tau^2(1+f)^2}. \tag{19}$$

This defines the restriction on the combinations of τ and E_0/n imposed by our number count, on the assumption that the expansion is described by the Sedov adiabatic expression—which appears to be so, at least out to a diameter of 32 pc ($\Sigma_{408} = 3 \times 10^{-20}$ W m^{-2} Hz^{-1} sr^{-1}).

Our N–D relation is shown in Fig. 4, where we use values of D given in Tables V and VI and plot equation (17) (with $f = 0$) as a solid line for $D < 32$ pc. We emphasize the considerable difference of our results from earlier work. For example, although the slope of Ilovaisky & Lequeux's (1972a, b) N–D relationship does not

Downloaded from https://academic.oup.com/mnras/article/174/2/267/1052695 by guest on 20 August 2022

© Royal Astronomical Society • Provided by the NASA Astrophysics Data System

1976MNRAS.174..267C

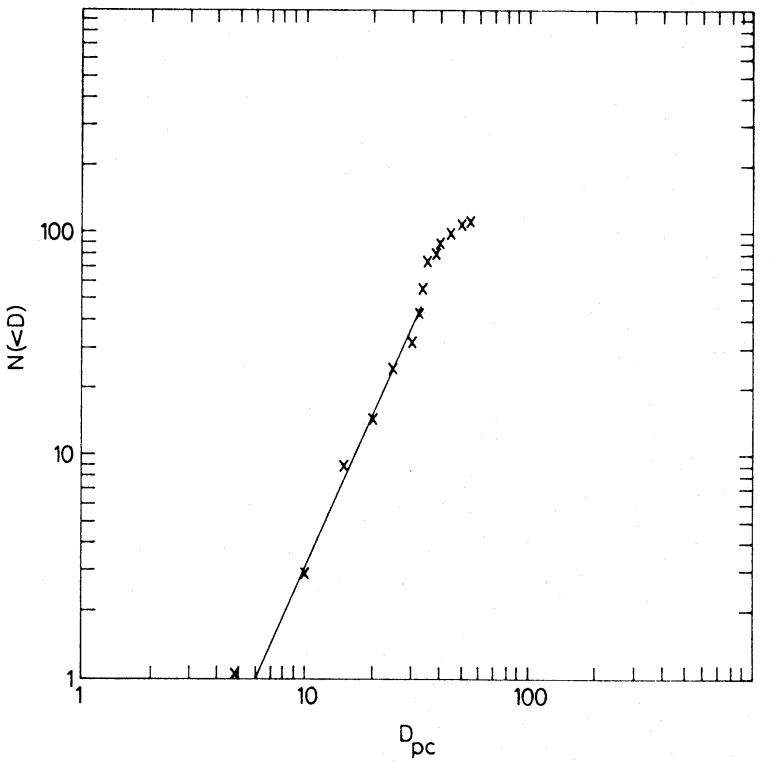

FIG. 4. *N–D relationship for the whole of the Galaxy.*

differ significantly from ours, the multiplying constant differs greatly; whereas they predict 170 SNRs with $D < 25$ pc, our Fig. 4 shows 26. This difference stems entirely from the fact that their distance scale is smaller than ours (by a factor of approximately 0·67 near $\Sigma_{408} = 10^{-19}$ W m^{-2} Hz^{-1} sr^{-1}) which, in addition to the direct effect, also led them to make large corrections for assumed incompleteness. The earlier results of Milne (1970) and Downes (1971) on which the Ilovaisky & Lequeux analysis is based, are similarly at variance with our results.

We will now attempt to estimate a rate of occurrence of supernova events and first review the three approaches which are available—all of them very similar.

(1) To assume that all ' recent ' supernovae (since Tycho's AD 1572 supernova say) have been recorded; an allowance may be made for the likelihood of distant events being unobserved because of obscuration. In addition to Tycho's and Kepler's supernovae we include Cas A, since it is almost certainly younger than either of these. This suggests an upper limit to the time interval between supernovae of about 130 yr. Katgert & Oort (1967) suggest a figure as low as 25 yr from this approach, making considerable allowance for obscuration.

(2) To assume that all SNRs with Σ greater than that for a suitable age calibrator are younger (e.g. Caswell 1970b). Kesteven's (1968b) method is a variant using a theoretical Σ–t relation rather than individual calibrators.

(3) To assume that all SNRs with diameter less than that of a remnant of known age are younger than this calibrator. Ilovaisky & Lequeux (1972b) have applied this technique to all currently available age calibrators, and conclude that $\tau = 50 \pm 25$ yr. In a variation used by Milne (1970), Downes (1971), and Mathewson & Clarke (1973), the theoretical (Sedov) D–t relation is assumed rather than any specific age calibrators. However, in this case a value for E_0/n must be estimated,

Downloaded from https://academic.oup.com/mnras/article/174/2/267/1052695 by guest on 20 August 2022

© Royal Astronomical Society • Provided by the NASA Astrophysics Data System

1976MNRAS.174..267C

and its choice is partly determined by the resulting ' predicted ' ages for remnants with independently known ages.

Methods (2) and (3) are identical only if both the diameters used in (3) are derived from the Σ's used in (2) *and* the age calibrator lies on (or is assumed to lie on) the mean Σ–D curve.

In principle, (2) might be preferred since it uses the observational data more directly than (3); however, because most of the SNRs above our completeness limit are apparently in the Sedov expansion phase, method (3) has the advantage that it allows other restrictions on E_0/n to be readily incorporated. We will ignore any distinction between Type 1 and Type 2 supernovae since there is no evidence of such a division in the radio remnants.

Tycho's and Kepler's supernovae will be used as principal calibrators; their diameters (13·8 and 9·3 pc respectively) and ages (403 and 371 yr respectively) inserted in equation (2) give values of E_0/n of 21×10^{51} and $3{\cdot}4 \times 10^{51}$ erg cm^3 respectively. (Minkowski (1968) obtained slightly different values owing to the different distance estimates and angular sizes which he used.) Inserted in equation (18) these remnants yield values of $\tau = 71/(1+f)$ and $176/(1+f)$ yr respectively. It has been argued (e.g. Ilovaisky & Lequeux 1972b) that both these remnants will have unusually low values of n at their large distances from the galactic plane and, since $\tau \propto n^{1/2}$, τ from either of them is an underestimate for a typical remnant. However, it seems unreasonable to increase τ much beyond ~ 130 yr in view of the known strong radio emitting remnants Tycho, Kepler and Cas A (and probably G349·7+0·2) which have clearly occurred quite recently. We will therefore draw on estimates of E_0/n from other information to investigate this further.

TABLE VII

Four X-ray SNRs and their inferred values of E_0/n

Name	Diameter (pc)	E_0/n (10^{50} erg cm^3)	z (pc)
G74·0−8·6 (Cyg Loop)	(38) 43·6	(27) 40	−120
G260·4−3·4 (Puppis A)	(17) 34·9	(5) 43	−148
G263·9−3·3 (Vela)	(40) 38·3	(50) 40	−29
G189·1+2·9 (Ic 443)	(20) 32·8	(24) 106	+142

Four of the SNRs which are too old to have been recorded historically show X-ray emission; they are the Cygnus Loop, Puppis A and Vela (Gorenstein, Harnden & Tucker 1974) and IC 443 (Winkler & Clark 1974). With several assumptions which are discussed by these authors, values for E_0/n may be estimated from the X-ray data and linear diameter. The estimates are summarized in Table VII. We quote in parentheses the diameters and resulting E_0/n values given in Gorenstein, Harnden & Tucker and Winkler & Clark, together with our estimates of diameter (from Tables V and VI, as discussed in the following section) and the resulting revised values of E_0/n (E_0/n scales as D^3). The X-ray data in all cases support E_0/n values of $\sim 5 \times 10^{51}$.

We now consider the choice of best mean estimates for E_0/n and τ; in Table VIII, corresponding values of E_0/n and τ, as constrained by our equation (19), are shown. Apart from Tycho's supernova all other calibrators suggest E_0/n values of $\sim 5 \times 10^{51}$; they as well as Tycho are at fairly large $|z|$ and might be

Downloaded from https://academic.oup.com/mnras/article/174/2/267/1052695 by guest on 20 August 2022

© Royal Astronomical Society • Provided by the NASA Astrophysics Data System

1976MNRAS.174..267C

TABLE VIII

Corresponding values of E_0/n and τ compatible with the experimental N–D relation

E_0/n (10^{50} erg cm^3)	τ (yr) if $f = 0$ (catalogue complete)	τ (yr) if $f = 0{\cdot}4$ (catalogue incomplete—see test)
424	50	25
188	75	37·5
106	100	50
47	150	75
26·5	200	100
6·6	400	200
1·7	800	400

expected to have low values of n, i.e. larger than average E_0/n. Thus there seems no evidence for an average interval less than $\tau \sim 150$ yr (if the catalogue is nearly complete—with a lower limit of ~ 75 yr if the catalogue were incomplete by 40 per cent). Values of τ significantly greater than 150 yr seem to be ruled out by the recent historically recorded remnants and thus we adopt as best estimates $\tau = 150$ yr, $E_0/n = 5 \times 10^{51}$ erg cm^3.

7. SNR EVOLUTION AS INDICATED BY THE OBSERVATIONS

We first summarize the set of relationships which result from equations (14) and (17) if we further assume that $\tau = 150$ yr and $E_0/n = 5 \times 10^{51}$ erg cm^3. They are:

$$\Sigma = 10^{-15} D^{-3},$$

$$D = 0{\cdot}93\, t^{2/5},$$

$$N = 8{\cdot}0 \times 10^{-3} D^{5/2},$$

$$N = 2{\cdot}53 \times 10^{-15} \Sigma^{-5/6},$$

$$\Sigma = 1{\cdot}25 \times 10^{-15} t^{-6/5}.$$

These we regard as applicable down to a 408 MHz surface brightness of 3×10^{-20} W m^{-2} Hz^{-1} sr^{-1}, indicating that, to this limit at least, the dynamical evolution is described by the Sedov expansion. Accordingly, the ages for remnants above this limit have been calculated from the Σ–t relation (the limiting age at $\Sigma_{408} = 3 \times 10^{-20}$ W m^{-2} Hz^{-1} sr^{-1} being ~ 7000 yr); values are given in Tables V and VI. The scatter in the Σ–D relation suggests that, for at least some SNRs, the estimated ages can be too great or too small by a factor of 2 or more.

We noted in Section 5 that there was an apparent steepening of the Σ–D relation near $\Sigma = 3 \times 10^{-20}$ W m^{-2} Hz^{-1} sr^{-1}. With the evolution summarized above, the expansion velocity at this value of Σ would still be nearly 1000 km s^{-1}. This is a factor of 5 higher than the value suggested by Woltjer (1972) as corresponding approximately to the transition from adiabatic to isothermal phases, and thus it appears that the Σ–D 'break' cannot be identified with this transition.

It should be pointed out that there are currently at least three different interpretations of the conditions present in old SNRs. Moffat (1971) suggests that in the Cygnus Loop (and probably other old remnants) the small velocities observed in the optical filaments represent expansion velocities and the corresponding age is

© Royal Astronomical Society • Provided by the NASA Astrophysics Data System

Downloaded from https://academic.oup.com/mnras/article/174/2/267/1052695 by guest on 20 August 2022

1976MNRAS.174..267C

$\sim 50\,000$ yr (see Minkowski 1968). High densities present in the filaments could then best be explained if the isothermal phase has been reached, since compressions much greater than in the adiabatic phase may be obtained. Such compressions might equally allow the radio emission to be generated by van der Laan's (1962) mechanism. In a second interpretation, other authors (e.g. Shklovsky 1974; Ilovaisky & Lequeux 1972b) accept the optical velocities and great ages but regard the remnants as still being in the adiabatic phase. The third interpretation not only regards the sources as being in the adiabatic phase but also much younger than implied by the optical velocities. This is the interpretation, first prompted by the X-ray data, which we have adopted earlier in Section 6. The velocities of the filaments are regarded as much lower than the expansion velocity, and a detailed investigation attributing these quasi-stationary features to encounters of the shock front with dense clouds has been presented by McKee & Cowie (1975). The high compression invoked to explain the optical emission might also allow van der Laan's model to explain the radio emission even in the adiabatic phase, but this aspect has not yet been investigated. Furthermore, DeNoyer (1975) finds that H I measurements around the Cygnus Loop can also be interpreted most readily on this third interpretation. Earlier we regarded the third interpretation as that most compatible with our N–D results, since it alone allows values of τ as small as 150 yr. It might be argued that values of $\tau > 150$ yr are not excluded by the frequency of young remnants if the origin of radio emission for young remnants differs from that of old remnants (in which case perhaps only a small fraction of remnants become bright in the later stages). Such an objection seems unwarranted in view of the apparently continuous distribution of sources along the Σ–D ' evolutionary ' track with steadily increasing numbers of older (larger D) remnants.

It seems appropriate here to discuss briefly two aspects of SNRs concerning their frequency and typical energies:

(i) We note that our rate, although slightly less than that derived in earlier studies, is still essentially the same (to within the large uncertainties) as current estimates of the rate of pulsar formation.

(ii) The rate of supply of kinetic energy to the interstellar medium has been discussed by Kahn & Woltjer (1967) and Woltjer (1970, 1972). Our results, suggesting typical values of E_0/n an order of magnitude greater than assumed in previous work, with a reduction by only a small factor in the rate of occurrence of supernovae, make it plausible that SNRs could indeed provide most of the energy to maintain the random motions of interstellar gas clouds, but the uncertainty in this latter energy requirement is necessarily large.

8. THE SPECTRAL INDEX

The distribution of spectral indices for SNRs in the range $l\ 180° \rightarrow 360°$, $D < 36$ pc, is shown in Fig. 5. This may be approximated by a normal distribution with mean value $-0{\cdot}45$, and standard deviation $\approx 0{\cdot}15$.

There is no indication that the spectral index is correlated with any other features of the SNR. Although the three young remnants Cas A, Tycho and Kepler all have spectra steeper than the average, there are other young (high-surface-brightness) SNRs with shallow spectra. The relatively steep spectrum of Cas A is flattening with time (Dent, Aller & Olsen 1974), but this does not appear

Downloaded from https://academic.oup.com/mnras/article/174/2/267/1052695 by guest on 20 August 2022

© Royal Astronomical Society • Provided by the NASA Astrophysics Data System

1976MNRAS.174..267C

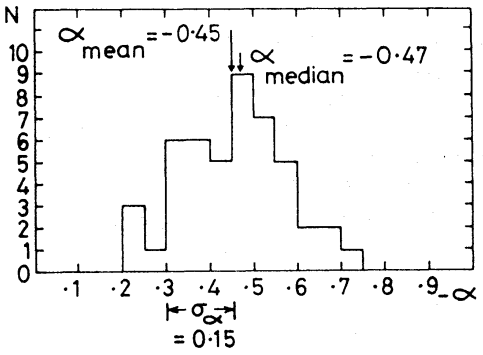

FIG. 5. *Spectral index distribution for SNRs with l* 180° → 360°, $D < 36$ *pc.*

to be a common evolutionary feature, since the average spectrum for low-surface-brightness SNRs is not significantly flatter than that for young remnants. Fig. 6 shows spectral index plotted as a function of linear diameter (being taken as an indicator of age), for the 97 SNRs from Tables I and II which we believe have the most reliable spectral index estimates. There does not appear to be any correlation between the two parameters.

Recently Becker & Kundu (1975) claim to have detected a relationship between spectral index and z-distribution but the significance of their result is questionable. We repeated the investigation using the estimates of α and z derived in the present paper and the trend noted by Becker & Kundu—SNRs with flatter spectra having a wider z-distribution—is not apparent. Any further investigation of this question would be better directed towards the individual remnants having large $|z|$ and flat α since they are quite few in number.

9. THE GALACTIC DISTRIBUTION OF SNRS

In Fig. 7, we have plotted the distribution, projected on to the galactic plane, of those SNRs from Tables V and VI having linear diameters less than 36 pc (corresponding to our surface-brightness confusion limit). The open and filled

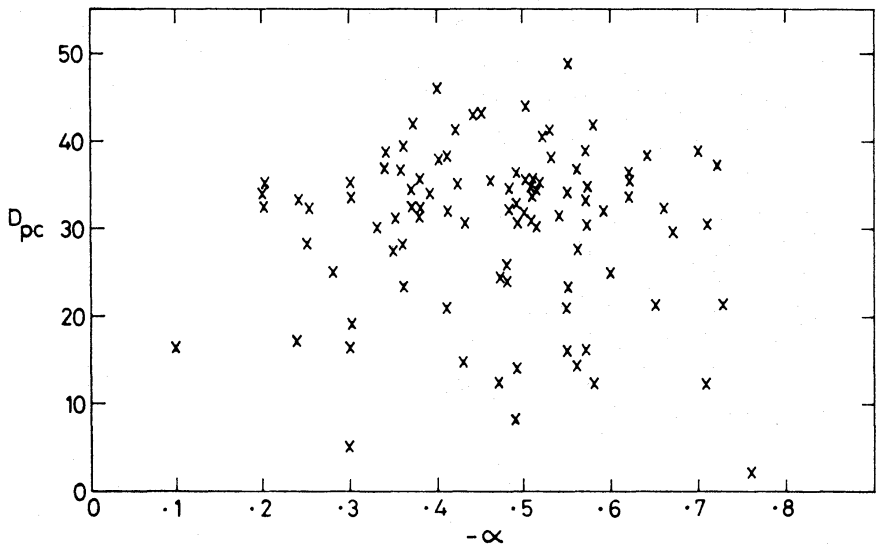

FIG. 6. *Spectral index as a function of linear diameter for all SNRs with well-determined α and D.*

Downloaded from https://academic.oup.com/mnras/article/174/2/267/1052695 by guest on 20 August 2022

© Royal Astronomical Society • Provided by the NASA Astrophysics Data System

1976MNRAS.174..267C

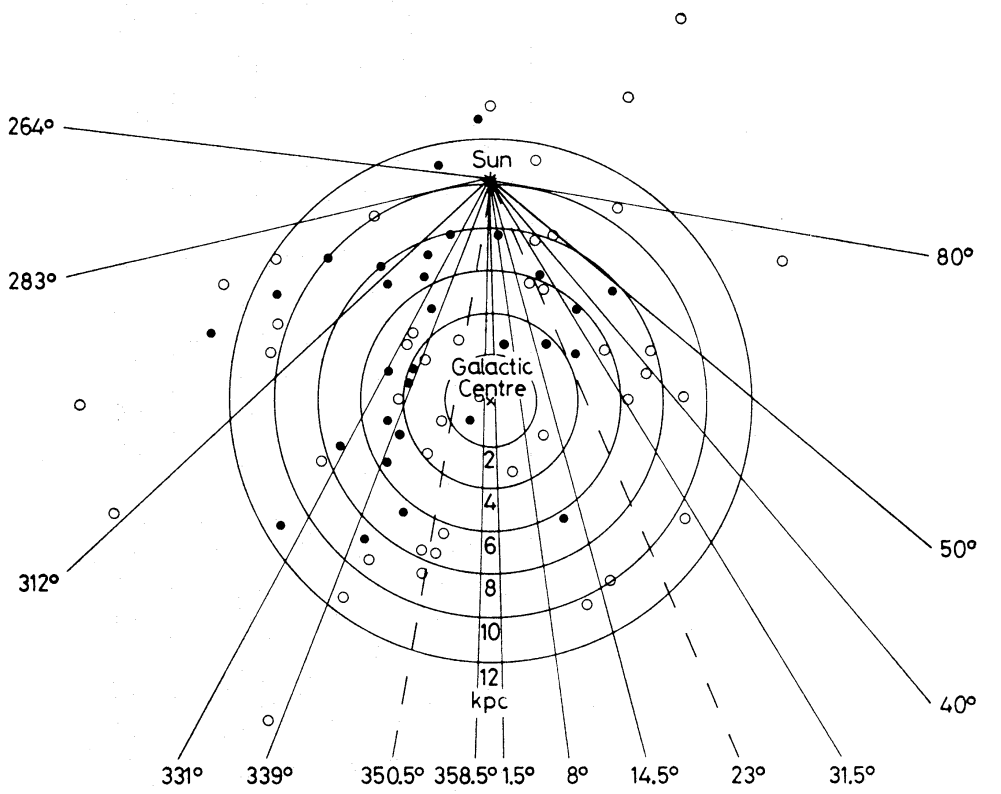

FIG. 7. *Galactic distribution for SNRs with $D < 36$ pc. Open circles denote younger remnants ($D < 32$ pc); filled circles denote older remnants of lower surface brightness and larger angular size. Solid lines are directions tangential to spiral arms; broken lines are possible tangential directions (from Green 1972).*

circles signify SNRs with distances estimated from equations (14) and (15) respectively. Because of the uncertainties in the distances to individual remnants (estimated as ~30 per cent in Section 5) it seems that SNRs can be used as spiral arm tracers only in so far as they indicate tangential points, for which direction rather than distance is important. Shown on Fig. 7 is the position of the ' tangent points ' in the galactic background radiation determined by Green (1972) from the Molonglo galactic survey. Our distribution of Fig. 7 possibly shows a concentration of SNRs in the direction of the tangent points, lending support to a Population I hypothesis with SNRs lying in the spiral arms.

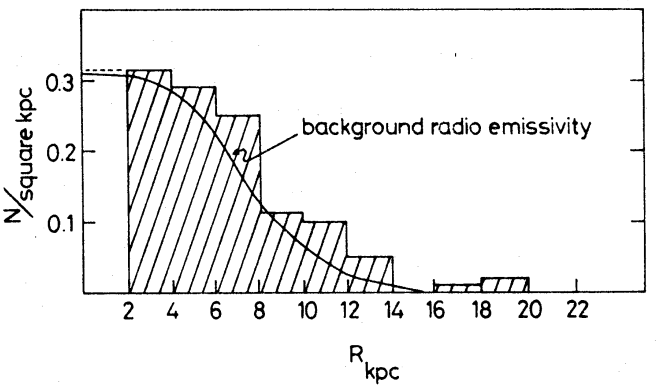

FIG. 8. *Surface density of SNRs in the galactic plane as a function of distance from the galactic centre, for l 180° → 360°.*

Downloaded from https://academic.oup.com/mnras/article/174/2/267/1052695 by guest on 20 August 2022

© Royal Astronomical Society • Provided by the NASA Astrophysics Data System

1976MNRAS.174..267C

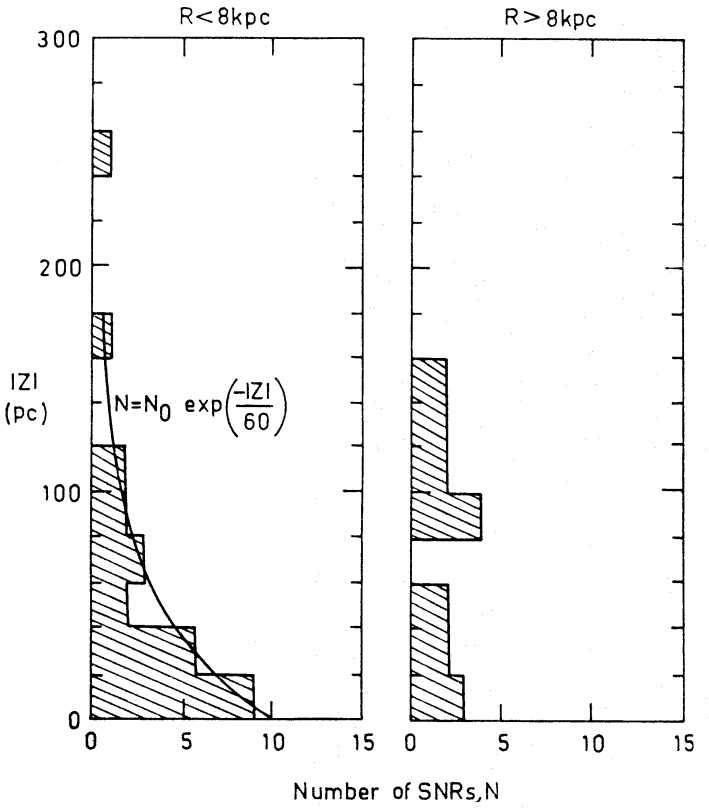

FIG. 9. *z distribution for SNRs with l* 180° → 360°, $|z| < 300$ *pc.*

The surface density of SNRs projected on to the galactic plane has been estimated using SNRs in the galactic longitude range 180° → 360° and with $D < 36$ pc (within these limits, we have argued that our catalogue is nearly complete). The surface density as a function of distance, R, from the galactic centre is plotted as Fig. 8. It is seen that SNRs are mainly concentrated to within little more than the solar distance. The distribution of SNRs follows closely the radial distribution of the non-thermal background radio emission evaluated by Ilovaisky & Lequeux (1972b), as shown in their Fig. 4 and superimposed on our Fig. 8.

The $|z|$-distributions of the SNRs are shown in Fig. 9 for $R < 8$ kpc and $R > 8$ kpc. Again we have imposed the limits l 180° → 360°, $D < 36$ pc; only 12 SNRs have $|z| > 300$ pc beyond the range of the diagrams. Within 8 kpc of the galactic centre, SNRs are concentrated close to the plane with a scale height of 60 pc; the $|z|$-distribution may be closely approximated by

$$N(z) = N(0) \exp(-|z|/60).$$

Beyond 8 kpc from the galactic centre, SNRs are no longer so strongly concentrated towards the plane. In this regard they are similar to the non-thermal background radio emission, and also to the neutral hydrogen, although the neutral hydrogen distribution extends very much further from the galactic centre than that for SNRs. The distributions of Fig. 9 have the same form as those of Ilovaisky & Lequeux (1972a), who noted similarities with the $|z|$-distribution parameters of extreme Population I objects.

Since in the adiabatic phase the time to reach a given diameter is proportional to $n^{1/2}$, the remnants of supernovae that exploded in regions of low interstellar density will have a comparatively short survival time. Shklovsky (1974) has there-

Downloaded from https://academic.oup.com/mnras/article/174/2/267/1052695 by guest on 20 August 2022

© Royal Astronomical Society • Provided by the NASA Astrophysics Data System

1976MNRAS.174..267C

fore argued that remnants in the galactic spiral arms could survive more than 10 times longer than those lying far from the galactic plane or between the spiral arms. Such a 'selection effect' might contribute to the apparent Population I bias of our SNR catalogue.

10. COMPARISON WITH THE MAGELLANIC CLOUDS

In Section 5 we found it valuable to use results on the Magellanic Cloud SNRs to interpret the galactic Σ–D relationship. Here we attempt to understand some anomalies in the Magellanic Cloud results using our galactic SNR results.

Mathewson & Clarke (1973) attempted to derive an $N(D)$–D relationship using 14 probable remnants in the Large Magellanic Cloud (their Fig. 12). One of the remnants used is probably spurious (Mills 1974) and we omit it. On the basis of the four brightest ($D < 10$ pc) remnants, Mathewson & Clarke predicted that about 340 SNRs should be detectable in the Large Magellanic Cloud above the sensitivity limit of the Molonglo cross ($\Sigma > 2 \times 10^{-21}$ W m^{-2} Hz^{-1} sr^{-1}), whereas only 13 were detected, all with $\Sigma > 10^{-20}$ W m^{-2} Hz^{-1} sr^{-1} ($D < 50$ pc). They pointed out that their $N(D)$–D relation would predict a supernova event once in 500 yr if it is assumed that $E_0/n = 10^{50}$ erg cm^3.

Thus two anomalies require explanation. Why have the large number of expected remnants not been detected? Is it reasonable that E_0/n should differ so greatly from our estimate for the Galaxy? Both anomalies are removed if we assume that the $N(D)$–D relation has been incorrectly estimated owing to the small number (4) of remnants used. If we assume the detections are complete to $\Sigma = 3 \times 10^{-20}$ W m^{-2} Hz^{-1} sr^{-1}, i.e. $D < 32$ pc (chosen because from our galactic results we suspect the Σ–D relation may steepen below this surface brightness), then we have nine Large Magellanic Cloud SNRs.

Since, according to our data, the Galaxy contains 50 SNRs brighter than this, it appears that the rate of occurrence in the Large Magellanic Cloud is smaller than in the Galaxy by the factor 9/50, suggesting a mean interval of 830 yr. This comparison which uses our galactic age calibration is equivalent to assuming that E_0/n for the Large Magellanic Cloud is on the average equal to 5×10^{51} erg cm^3, as was inferred for the Galaxy; the interval obtained for the Magellanic Clouds would be reduced by a factor of 2 if either E_0 were larger by a factor of 4, or n were smaller by a factor of 4, or the number of detected Magellanic Cloud remnants were erroneously low by a factor of 2 owing either to undetected remnants or statistical fluctuations.

It appears that with the above explanation there is no need to postulate values of E_0/n differing greatly from those in the Galaxy, and the mystery of the missing remnants is also solved. It is, however, necessary to postulate that the excess (~ 3) of small-diameter Magellanic Cloud remnants is merely a statistical fluctuation; on current evidence this seems the most plausible explanation.

11. CONCLUSIONS

The general evolutionary properties of galactic SNRs have been investigated using improved observational data. In Section 6 we found that the dynamical evolution appears to correspond to an adiabatic expansion, at least down to the surface brightness limit of the catalogue.

Completeness in the catalogue of SNRs to a uniform low level of surface bright-

Downloaded from https://academic.oup.com/mnras/article/174/2/267/1052695 by guest on 20 August 2022

© Royal Astronomical Society • Provided by the NASA Astrophysics Data System

1976MNRAS.174..267C

ness has permitted an improved estimate of the number of SNRs in the Galaxy, which suggests that this number has previously been overestimated. A consequence of this conclusion is that the 'characteristic interval' between supernova events of a kind which produce typical remnants is ~ 150 yr—somewhat larger than previous estimates but still comparable with estimates of pulsar birth-rates. In addition, on the assumption that most of the brighter SNRs are in the Sedov adiabatic expansion phase, the typical value of E_0/n implied by our data is 5×10^{51} erg cm^3—higher than commonly assumed in earlier work, but in agreement with estimates based on recent X-ray observations.

The $|z|$ distribution of SNRs, their concentration at longitudes showing peaks in the galactic background radiation (probably spiral-arm tangent points), and their concentration mainly within little more than the solar distance from the galactic centre, are all similar to the distribution of extreme Population I objects. In Section 5 we found that the relationship between surface brightness and linear diameter (Σ–D) for the galactic SNRs does not differ from that determined for the Magellanic Clouds contrary to earlier conclusions; further comparisons with the Magellanic Clouds in Section 10 help to resolve puzzling differences between the properties of SNRs in the Galaxy and the Magellanic Clouds suggested by previous work.

The Σ–D approach is at present an empirical one with little theoretical foundation, but the quality of present observational data and their statistical implications provide valuable constraints against which future theoretical models may be tested.

ACKNOWLEDGMENTS

We thank Professor B. Y. Mills and Dr B. J. Robinson for suggesting this Molonglo–Parkes collaborative study.

REFERENCES

Aizu, K. & Tabara, H., 1967. *Prog. theor. Phys., Japan*, **37**, 296.
Balona, L. A. & Feast, M. W., 1974. *Mon. Not. R. astr. Soc.*, **167**, 621.
Beard, M., 1966. *Aust. J. Phys.*, **19**, 141.
Becker, R. H. & Kundu, M. R., 1975. *Astr. Astrophys.*, **38**, 149.
Berkhuijsen, Elly M., 1974. *Astr. Astrophys.*, **35**, 429.
Bolton, J. G., Gardner, F. F. & Mackey, M. B., 1964. *Aust. J. Phys.*, **17**, 340.
Caswell, J. L., 1967. *Mon. Not. R. astr. Soc.*, **136**, 11.
Caswell, J. L., 1970a. *Aust. J. Phys.*, **23**, 105.
Caswell, J. L., 1970b. *Astr. Astrophys.*, **7**, 59.
Caswell, J. L., 1972. *Aust. J. Phys.*, **25**, 443.
Caswell, J. L. & Clark, D. H., 1975. *Aust. J. Phys. Astrophys. Suppl. No.* **37**, 57.
Caswell, J. L., Clark, D. H. & Crawford, D. F., 1975. *Aust. J. Phys. Astrophys. Suppl. No.* **37**, 39.
Caswell, J. L. & Goss, W. M., 1970. *Astrophys. Lett.*, **7**, 142.
Caswell, J. L. & Haynes, R. F., 1975. *Mon. Not. R. astr. Soc.*, **173**, 649.
Caswell, J. L., Dulk, G. A., Goss, W. M., Radhakrishnan, V. & Green, Anne J., 1971. *Astr. Astrophys.*, **12**, 271.
Caswell, J. L., Murray, J. D., Roger, R. S., Cole, D. J. & Cooke, D. J., 1975. *Astr. Astrophys.*, in press.
Chevalier, R. A., 1974. *Astrophys. J.*, **188**, 501.
Clark, D. H. & Crawford, D. F., 1974. *Aust. J. Phys.*, **27**, 713.
Clark, D. H., Caswell, J. L. & Green, Anne J., 1973. *Nature*, **246**, 28.
Clark, D. H., Caswell, J. L. & Green, Anne J., 1975a. *Aust. J. Phys. Astrophys. Suppl. No.* **37**, 1.

Downloaded from https://academic.oup.com/mnras/article/174/2/267/1052695 by guest on 20 August 2022

© Royal Astronomical Society • Provided by the NASA Astrophysics Data System

1976MNRAS.174..267C

Clark, D. H., Green, Anne J. & Caswell, J. L., 1975b. *Aust. J. Phys. Astrophys. Suppl. No.* **37,** 75.
Crawford, D. F. Jauncey, D. L. & Murdoch, H. S., 1970. *Astrophys. J.*, **162,** 405.
Crowther, J. H., 1965. *Observatory*, **85,** 946.
Day, G. A., Caswell, J. L. & Cooke, D. J., 1972. *Aust. J. Phys. Astrophys. Suppl. No.* **25,** 1.
DeNoyer, L. K., 1975. *Astrophys. J.*, **196,** 479.
Dent, W. A., Aller, H. D. & Olsen, E. T., 1974. *Astrophys. J. Lett.*, **188,** L11.
Dickel, J. R., 1969. *Astrophys. Lett.*, **4,** 109.
Dickel, J. R., McGuire, J. P. & Yang, K. S., 1965. *Astrophys. J.*, **142,** 798.
Dickel, J. R. & McKinley, R. R., 1969. *Astrophys. J.*, **155,** 67.
Dickel, J. R. & Milne, D. K., 1972. *Aust. J. Phys.*, **25,** 539.
Dickel, J. R. & Yang, K. S., 1965. *Astrophys. J.*, **142,** 1642.
Downes, D., 1971. *Astr. J.*, **76,** 305.
Downes, D. & Wilson, T. L., 1974. *Astr. Astrophys.*, **34,** 133.
Duin, R. M., Israel, F. P., Dickel, J. R. & Seaquist, E. R., 1975. *Astr. Astrophys.*, **38,** 461.
Erkes, J. W. & Dickel, J. R., 1969. *Astr. J.*, **74,** 840.
Gorenstein, P., Harnden, F. R. & Tucker, W. H., 1974. *Astrophys. J.*, **192,** 661.
Goss, W. M. & Day, G. A., 1970. *Aust. J. Phys. Astrophys. Suppl. No.* **13,** 3.
Goss, W. M., Radhakrishnan, V., Brooks, J. W. & Murray, J. D., 1972. *Astrophys. J. Suppl.*, **24,** 123.
Goss, W. M. & Schwarz, U. J., 1971. *Nature Phys. Sci.*, **234,** 52.
Goss, W. M., Schwarz, U. J. & Wesselius, P. R., 1973. *Astr. Astrophys.*, **28,** 305.
Goss, W. M. & Shaver, P. A., 1970. *Aust. J. Phys. Astrophys. Suppl. No.* **14,** 1.
Green, Anne J., 1971. *Aust. J. Phys.*, **24,** 773.
Green, Anne J., 1972. *PhD Thesis*, University of Sydney.
Green, Anne J., 1974. *Astr. Astrophys. Suppl.*, **18,** 325.
Gull, S. F., 1973. *Mon. Not. R. astr. Soc.*, **161,** 47.
Gull, S. F., 1975. *Mon. Not. R. astr. Soc.*, **171,** 237.
Harris, D. E., 1962. *Astrophys. J.*, **135,** 661.
Haslam, C. G. T. & Salter, C. J., 1971. *Mon. Not. R. astr. Soc.*, **151,** 385.
Haslam, C. G. T., Wilson, W. E., Graham, D. A. & Hunt, G. C., 1974. *Astr. Astrophys. Suppl.*, **13,** 359.
Higgs, L. A. & Halperin, W., 1968. *Mon. Not. R. astr. Soc.*, **141,** 209.
Hill, E. R., 1967. *Aust. J. Phys.*, **20,** 297.
Hill, I. E., 1972. *Mon. Not. R. astr. Soc.*, **157,** 419.
Hill, I. E., 1973. *Mon. Not. R. astr. Soc.*, **164,** 39P.
Hill, I. E., 1974. *Mon. Not. R. astr. Soc.*, **169,** 59.
Holden, D. J., 1968. *Mon. Not. R. astr. Soc.*, **141,** 57.
Holden, D. J. & Caswell, J. L., 1969. *Mon. Not. R. astr. Soc.*, **143,** 407.
Ilovaisky, S. A. & Lequeux, J., 1972a. *Astr. Astrophys.*, **18,** 169.
Ilovaisky, S. A. & Lequeux, J., 1972b. *Astr. Astrophys.*, **20,** 347.
Jones, B. B., 1973. *Aust. J. Phys.*, **26,** 545.
Jones, B. B. & Finlay, E. A., 1974. *Aust. J. Phys.*, **27,** 687.
Kahn, F. D. & Woltjer, L., 1967. In *Radio astronomy and the galactic system*, IAU Symp. 31, p. 117, ed. Hugo van Woerden, Academic Press, London.
Katgert, P. & Oort, J. H., 1967. *Bull. astr. Inst. Nethl.*, **19,** 239.
Keen, N. J., Wilson, W. E., Haslam, C. G. T., Graham, D. A. & Thomasson, P., 1973. *Astr. Astrophys.*, **28,** 197.
Kellermann, K. I., Pauliny-Toth, I. I. K. & Williams, P. J. S., 1969. *Astrophys. J.*, **157,** 1.
Kesteven, M. J. L., 1968a. *Aust. J. Phys.*, **21,** 369.
Kesteven, M. J. L., 1968b. *Aust. J. Phys.*, **21,** 739.
Kundu, M. R., 1971. *Astrophys. J. Lett.*, **165,** L55.
Kundu, M. R. & Becker, R. H., 1972. *Astr. J.*, **77,** 459.
Kundu, M. R. & Velusamy, T., 1967. *Ann. Astrophys.*, **30,** 723.
Kundu, M. R. & Velusamy, T., 1969. *Astrophys. J.*, **155,** 807.
Kundu, M. R. & Velusamy, T., 1971a. *Astrophys. J.*, **163,** 231.
Kundu, M. R. & Velusamy, T., 1971b. *Nature Phys. Sci.*, **234,** 54.
Kundu, M. R. & Velusamy, T., 1972. *Astr. Astrophys.*, **20,** 237.

Downloaded from https://academic.oup.com/mnras/article/174/2/267/1052695 by guest on 20 August 2022

© Royal Astronomical Society • Provided by the NASA Astrophysics Data System

1976MNRAS.174..267C

Kundu, M. R., Velusamy, T. & Hardee, P. E., 1974. *Astr. J.*, **79,** 132.
Little, A. G., 1974. In *Galactic radio astronomy*, IAU Symp. No. 60, p. 491, eds F. J. Kerr & S. C. Simonson III, Reidel, Holland.
McKee, C. F. & Cowie, L. L., 1975. *Astrophys. J.*, **195,** 715.
Mathewson, D. S. & Clarke, J. N., 1973. *Astrophys. J.*, **180,** 725.
Mills, B. Y., 1974. In *Galactic radio astronomy*, IAU Symp. No. 60, p. 311, eds F. J. Kerr & S. C. Simonson, Reidel, Holland.
Mills, B. Y., Aitchison, R. E., Little, A. G. & McAdam, W. B., 1963. *Proc. Inst. Radio Engrs. Aust.*, **24,** 156.
Milne, D. K., 1968. *Aust. J. Phys.*, **21,** 201.
Milne, D. K., 1969. *Aust. J. Phys.*, **22,** 613.
Milne, D. K., 1970. *Aust. J. Phys.*, **23,** 425.
Milne, D. K., 1971a. *Aust. J. Phys.*, **24,** 429.
Milne, D. K., 1971b. *Aust. J. Phys.*, **24,** 757.
Milne, D. K., 1972. *Astrophys. Lett.*, **11,** 167.
Milne, D. K. & Dickel, J. R., 1971. *Nature Phys. Sci.*, **231,** 33.
Milne, D. K. & Dickel, J. R., 1975. *Aust. J. Phys.*, **28,** 209.
Milne, D. K. & Hill, E. R., 1969. *Aust. J. Phys.*, **22,** 211.
Milne, D. K. & Wilson, T. L., 1971. *Astr. Astrophys.*, **10,** 220.
Milne, D. K., Wilson, T. L., Gardner, F. F. & Mezger, P. G., 1969. *Astrophys. Lett.*, **4,** 121.
Minkowski, R., 1958. *Rev. mod. Phys.*, **30,** 1048.
Minkowski, R., 1966. *Astr. J.*, **71,** 371.
Minkowski, R., 1968. In *Nebulae and interstellar matter* (*Stars and stellar systems*, Vol. 7), p. 623, eds B. M. Middlehurst & L. H. Aller, University Chicago Press.
Moffat, P. H., 1971. *Mon. Not. R. astr. Soc.*, **153,** 401.
Radhakrishnan, V., Goss, W. M., Murray, J. D. & Brooks, J. W., 1972. *Astrophys. J. Suppl. Ser.*, **24,** 49.
Rosenberg, I., 1970. *Mon. Not. R. astr. Soc.*, **151,** 109.
Rosenberg, I. & Scheuer, P. A. G., 1973. *Mon. Not. R. astr. Soc.*, **161,** 27.
Sato, F., 1973. *Publ. astr. Soc. Japan*, **25,** 135.
Sedov, L. I., 1959. *Similarity and dimensional methods in mechanics*, Academic Press.
Shaver, P. A., 1969. *Mon. Not. R. astr. Soc.*, **142,** 273.
Shaver, P. A. & Goss, W. M., 1970a. *Aust. J. Phys. Astrophys. Suppl. No.* **14,** 77.
Shaver, P. A. & Goss, W. M., 1970b. *Aust. J. Phys. Astrophys. Suppl. No.* **14,** 133.
Shklovsky, I. S., 1960a. *Sov. Astr.*, **4,** 243.
Shklovsky, I. S., 1960b. *Sov. Astr.*, **4,** 355.
Shklovsky, I. S., 1962. *Sov. Astr.*, **6,** 162.
Shklovsky, I. S., 1968. *Supernovae*, Wiley-Interscience, London, 444 pp.
Shklovsky, I. S., 1974. *Sov. Astr.*, **18,** 1.
Slee, O. B. & Dulk, G. A., 1974. In *Galactic radio astronomy*, IAU Symp. No. 60, p. 347, eds F. J. Kerr & S. C. Simonson, Reidel, Holland.
Stankevich, K. S., Ivanov, V. P. & Torkhov, V. A., 1973. *Sov. Astr.*, **17,** 410.
Strom, R. G. & Duin, R. M., 1973. *Astr. Astrophys.*, **25,** 351.
Trimble, V., 1968. *Astr. J.*, **73,** 535.
van den Bergh, S., 1971. *Astrophys. J.*, **168,** 37.
van den Bergh, S. & Dodd, W. W., 1970. *Astrophys. J.*, **162,** 485.
van der Laan, H., 1962. *Mon. Not. R. astr. Soc.*, **124,** 179.
Velusamy, T. & Kundu, M. R., 1974. *Astr. Astrophys.*, **32,** 375.
Weiler, K. W. & Seielstad, G. A., 1971. *Astrophys. J.*, **163,** 455.
Wendker, H., 1968. *Z. Astrophys.*, **69,** 392.
Westerlund, B. E., 1969. *Astr. J.*, **74,** 879.
Whiteoak, J. B. & Gardner, F. F., 1968. *Astrophys. J.*, **154,** 807.
Williams, D. R. W., 1973. *Astr. Astrophys.*, **28,** 309.
Willis, A. G., 1973. *Astr. Astrophys.*, **26,** 237.
Willis, A. G. & Dickel, J. R., 1971. *Astrophys. Lett.*, **8,** 203.
Wilson, T. L., 1970. *Astrophys. Lett.*, **1,** 95.
Wilson, T. L., 1972. *Astr. Astrophys.*, **19,** 354.
Winkler, P. F. & Clark, G. W., 1974. *Astrophys. J. Lett.*, **191,** L67.

Downloaded from https://academic.oup.com/mnras/article/174/2/267/1052695 by guest on 20 August 2022

© Royal Astronomical Society • Provided by the NASA Astrophysics Data System

1976MNRAS.174..267C

Woltjer, L., 1970. In *Interstellar gas dynamics*, IAU Symp. No. 39, p. 299, ed. H. J. Habing, Reidel, Holland.
Woltjer, L., 1972. *A. Rev. Astr. Astrophys.*, **10**, 129.
Wyllie, D. V., 1969. *Mon. Not. R. astr. Soc.*, **142**, 229.
Wynn-Williams, C. G., Downes, D. & Wilson, T. L., 1971. *Astrophys. Lett.*, **9**, 113.
Yang, K. S. & Dickel, J. R., 1965. *Astr. J.*, **70**, 300.

Downloaded from https://academic.oup.com/mnras/article/174/2/267/1052695 by guest on 20 August 2022

© Royal Astronomical Society • Provided by the NASA Astrophysics Data System